

Production and Propagation of the Jupiter Radio Signal in the Jovian Magnetosphere

Elliot Devon-Hurley - 18319184

Supervisors: Dr. Corentin Louis and Prof. Caitriona Jackman



Trinity College Dublin
Coláiste na Tríonóide, Baile Átha Cliath
The University of Dublin

DIAS

Institiúid Ard-Léinn | Dublin Institute for
Bhaile Átha Cliath | Advanced Studies

Bachelor's Thesis - Senior Sophister Physics and Astrophysics 2021

School of Physics - Trinity College Dublin

Abstract

The aim of this study was to investigate the behaviour of Jovian narrowband kilometric radio emission (nKom) during periods of magnetospheric compression using the data collected by the Juno spacecraft. Using the findings from Hospodarsky et al. (2017), in conjunction with the Joy et al. model, four periods of magnetospheric compression have been identified during Juno's approach and first three orbits of Jupiter. It is found that the compression of the Jovian magnetosphere by the solar wind results in the activation of nKom sources. The emissions observed during compression typically occur in bursts, with two or three bursts observed throughout a compression period. The emissions display a ten-hour periodicity which indicates that the emission source is longitudinally fixed and rotating with Jupiter. In addition to this, nKom emissions are observed to change frequency after several rotations which is believed to be as a result of the emission source moving to areas of higher or lower plasma density inside the Io torus. From the findings in this study, it is concluded that observations of nKom emission may be used as a proxy for solar wind conditions at Jupiter.

Acknowledgements

My sincerest thanks to Prof. Caitriona Jackman and Dr. Corentin Louis, who invited me to conduct this research project at the Dublin Institute for Advanced Studies. Their continued guidance, encouragement and support has been invaluable.

Contents

1	Introduction	1
2	Theory and Background	2
2.1	The Solar Wind	2
2.1.1	Dynamic Pressure	2
2.2	Jupiter's Magnetosphere	4
2.2.1	The Magnetospheric boundaries	5
2.2.2	Io torus and the Plasmashell	6
2.2.3	Coordinate Systems	7
2.3	Jovian Radio Emission	8
2.3.1	The Components of the Jovian Radio Emission	8
3	Computational Method	10
3.1	Identifying Boundary Crossings	10
3.1.1	Juno's Orbital Path	11
3.2	Autoplot - Dynamic Spectra	13
3.3	nKom Time series	14
3.4	The Joy et al. Model	15
3.4.1	Using the Joy et al. Model for Boundary Crossings	16
4	Results and Discussion	17
4.1	Statistical Analysis of Boundary Crossings	17
4.1.1	Distance from Jupiter's Surface	17
4.1.2	Dynamic Pressure	18
4.2	Determination of Magnetospheric Compression Periods	20
4.3	nKom Emission During Magnetospheric Compression	21
4.4	Discussion of Results	27
5	Conclusions	30
6	References	31
7	Appendices	33

7.1	A - Boundary Crossing Determination	33
7.2	B - Initial Juno Orbital Path XZ Plane	33
7.3	C - An Example of the Joy et al. Model Creating Surfaces	34
7.4	D - Initial Juno Orbital Path in Three Dimensions	35
7.5	E - nKom Emission for 1st Compression Period DOY 180 - 182	36
7.6	F - Second Burst of Emission During the Second Identified Compression .	37
7.7	G - First Burst of Emission During the Third Identified Compression . .	37
7.8	H - Third Burst of Emission During the Third Identified Compression . .	38
7.9	I - Time Series for Second Emission During Third Compression From DOY 256 to DOY 258	38
7.10	J - nKom Emission During Fourth Compression DOY 276 - 297	39

1 Introduction

The magnetosphere of a planet is the area of space around a planet that is under the influence of the planet's magnetic field. The gas giant Jupiter is by far the largest planet in the solar system, and also possesses the largest and strongest magnetosphere. In order to study the Jovian atmosphere and magnetosphere, NASA launched the Juno satellite from Cape Canaveral in 2011, which completed Jupiter orbit insertion (JOI) on the 5th of July 2016.

The aim of this project is to use the data that has been gathered from this mission so far, to explore the mechanics of the magnetosphere and in turn, determine how these mechanics affect the radio emission that has long been observed from the gas giant. On-board the Juno satellite is a magnetometer that measures the magnetic field, and a Waves instrument that measures the radio emission. Using the magnetometer to measure the strength of the magnetic field as the spacecraft orbits the planet, it is possible to establish when the satellite crosses boundaries of the Jovian magnetosphere (Hospodarsky et al., 2017). The two key boundaries are the bow shock and the magnetopause. The magnetopause is the boundary that separates the solar wind from the magnetosphere. The bow shock is further upwind and is formed as a result of the sudden slowing of the solar wind as it encounters the magnetopause. The location of the magnetopause and hence the bow shock is determined by a pressure balance between the external solar wind against the internal planetary field. Due to the rotation of the Sun and variations in solar activity, the solar wind speed and pressure are subject to change which causes the pressure balance to change and thus cause movement of the boundaries of the magnetosphere (Joy et al., 2002). Periods of increased solar wind dynamic pressure cause the magnetosphere to become compressed and thus, the Juno spacecraft crosses the boundaries closer to Jupiter's surface than it would when the magnetosphere was in a relaxed state. The aim of this study is to examine the Jovian radio emission during these periods of compression to infer the relationship between the emissions and the solar wind dynamic pressure.

The radio emission of Jupiter can itself be broken into several components (see section 2.3.1). This study will investigate the effects of magnetospheric compression on one of these components by analysing the intensity and periodicity of the emission before, during and after a compression.

2 Theory and Background

2.1 The Solar Wind

The solar wind is created in the upper atmosphere of the Sun, known as the solar corona. Temperatures in the solar corona are in excess of one million degrees Celsius, and as a result, the plasma in this region has enough energy to escape the Sun's gravity and travel outward from the Sun along the Sun's magnetic field lines.(The Sun's Corona — Center for Science Education, 2012). As the Sun rotates (with a period of approximately 27 days) the magnetic fields rotate with it causing the flow of plasma known as the solar wind. As the solar wind travels outwards it carries with it, the end of the solar magnetic field lines which leads to the creation of the interplanetary magnetic field (IMF). As the solar wind is generated in the solar corona, its characteristics vary according to the solar cycle. The solar cycle alternates from solar minimum to solar maximum approximately every 11 years, with minimum and maximum being determined by the number of sunspots on the solar surface. During solar minimum, the IMF is typically orientated outward in the northern hemisphere and inward in the southern hemisphere, with faster solar wind velocities at higher latitudes and slower velocities nearer the equator. During solar maximum this is not the case; there is no pattern between inward and outward IMF or the solar wind velocities. As of 2016/2017 the number of sunspots on the surface of the Sun has been decreasing, meaning that during this study the Sun was approaching solar minimum.

Coronal mass ejections (CME's), occur when twisted solar magnetic field lines suddenly re-orientate in order to release some of the built up energy from the old configuration. This process is known as magnetic reconnection (NOAA / NWS Space Weather Prediction Center, 2017). This release of energy is the cause of CME's. CME's cause a shock in the solar wind and can increase the solar wind pressure resulting in the compression of a planet's magnetosphere.

2.1.1 Dynamic Pressure

When the solar wind encounters the magnetosphere of a planet, a pressure is applied to said magnetosphere. It is the variation in this pressure that causes the compression and

rarefaction of a magnetosphere. This pressure is called the solar wind dynamic pressure (P_{dyn}). The key measurables that affect the dynamic pressure are the solar wind speed and density. It is given by the following equation:

$$P_{dyn} = m_p N_p V_{sw}^2 \quad (1)$$

(Hess, Echer and Zarka, 2012). Where m_p is the proton mass, N_p is the proton density in cm^{-3} and V_{sw} is the solar wind velocity. In addition to the dynamic pressure, there are other solar wind parameters that are important to consider. The plasma beta is defined as the ratio between the plasma pressure and the magnetic pressure exerted by the magnetosphere of a planet. The beta of a plasma is given by:

$$\beta = \frac{2\mu_0 n k_b T}{B^2} \quad (2)$$

(Joy et al., 2002). Where μ_0 is the permeability constant, n is the density, k_b is the Boltzmann constant, T is the temperature and B is the magnetic field strength. The mach number of a fluid (or plasma) represents the velocity of the fluid as it flows past an obstacle. More precisely, it represents this velocity in relation to the local speed of sound. The mach number of a fluid is given by the following:

$$M = \frac{v}{c} \quad (3)$$

Here v is the velocity of the fluid around the boundary and c is the local speed of sound (Young, 2011). In terms of the solar wind, the sonic mach number describes the speed that the solar wind flows around the magnetopause in terms of the speed of sound. Additionally to the sonic mach number, the Alfvén mach number (M_A) relates the flow speed to the speed of Alfvén waves. Alfvén waves are a form of transverse magnetohydrodynamic wave that occur in plasmas due to the presence of a magnetic field (Bridgman, 2017). As the plasma moves in the magnetic field, it generates an EMF and thus electric currents are created. The interaction of these currents and the magnetic field gives rise to mechanical

forces that will change the motion of the plasma. (Alfvén, 1942). The speed of an Alfvén wave is given by:

$$V_A = \left(\frac{B^2}{\mu_0 \rho} \right)^{\frac{1}{2}} \quad (4)$$

(Ryden, 2009). Here B is the magnetic field strength, μ_0 is the vacuum permeability and ρ is the plasma density. It should be noted that, in terms of the sonic and Alfvénic mach numbers, the solar wind is both supersonic and superAlfvénic.

2.2 Jupiter's Magnetosphere

Different conditions cause the notable magnetospheres of the solar system to vary from one another to a large degree. Factors such as the planetary field strength, planetary rotation rate, upstream solar wind conditions, and the internal plasma conditions all affect the strength, size and shape of a magnetosphere. The magnetosphere of Jupiter is the largest object in the solar system. It stretches millions of kilometres in the sunward direction and has a long tail that can extend to the orbit of Saturn. The planet Jupiter is mostly composed of hydrogen and helium, however, as the pressures in Jupiter's core and mantle are sufficiently strong, the hydrogen can be compressed and form metallic hydrogen. This metallic hydrogen has similar conductivity to other known metals and thus, allows current to flow and a magnetosphere to form (Jones, 2018). The magnetosphere of Jupiter also has significant internal plasma activity. A disk of rotating plasma encompasses Jupiter owing to its volcanic satellite Io. The presence of this disk, combined with the fact that Jupiter is a fast rotator (having a rotational period of approximately 10 hours), creates an interesting internal plasma dynamic, which will be described later in this section. The size and shape of the Jovian magnetosphere is subject to change. Changes in different parameters of the solar wind can cause periods of compression and rarefaction in the magnetosphere. The focus of this study is to discern when these compression periods occur and to analyse the effects they have on the Jovian radio emission.

2.2.1 The Magnetospheric boundaries

Magnetospheres are divided into three key sections which are separated by two boundaries. As the solar wind approaches a magnetosphere, it encounters a boundary which it cannot penetrate due to the interaction of the solar wind's magnetic field and that of the magnetosphere. This boundary is known as the magnetopause. When the solar wind meets the magnetopause, its speed drops suddenly. This creates a shock further upstream of the magnetopause which is known as the bow shock. The bow shock separates the undisturbed solar wind from the magnetosheath. Both of these boundaries are shown below in Figure 1.

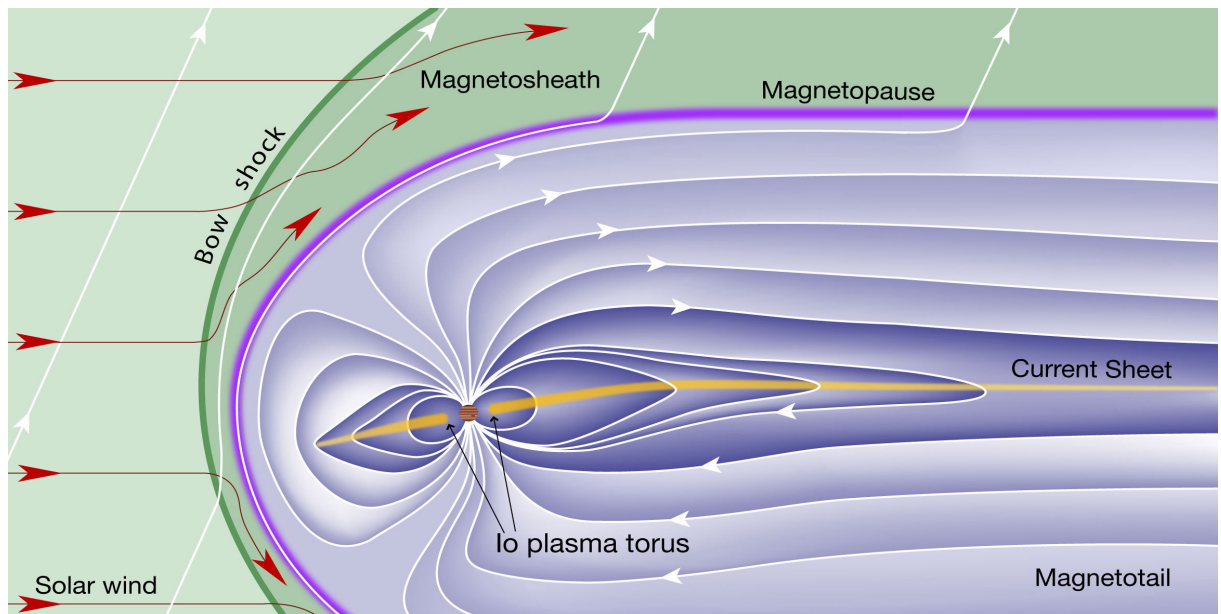


Figure 1: An image of Jupiter's magnetosphere with the key boundaries (bow shock and magnetopause) labelled (Bagenal and Bartlett).

The magnetosheath is the area between the bow shock and the magnetopause, it is composed of the slowed and compressed solar wind after it has initially encountered the bow shock. The second key boundary is the aforementioned magnetopause. The magnetopause is the boundary that separates the magnetosheath from the magnetosphere itself. The location of the magnetopause boundary is determined by the pressure balance of the external solar wind against the internal planetary field. As a result of a constantly changing solar wind, this pressure balance is constantly changing, and as a result, so is the location of the magnetopause and bow shock. In the context of this study, a paper published by Joy et al. (2002), determined that the standoff distance of the magnetopause boundary at Jupiter had a bimodal distribution, and that the most probable standoff dis-

tances are at $63 R_J$ and $92 R_J$. The paper also determined that the mean bow shock standoff distance was at $92 R_J$. These values correspond to the standoff distances which are measured at the "nose" of the magnetosphere. This is the section of the magnetosphere that is facing the sun and is the point at which the solar wind first encounters the magnetosphere.

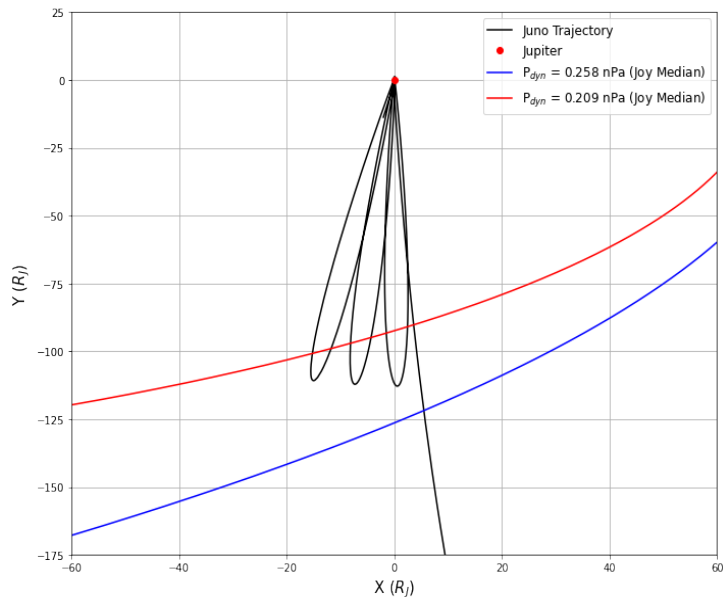


Figure 2: The trajectory of the Juno spacecraft (black line), and the median positions of the magnetopause and bow shock (red and blue lines respectively) predicted by the Joy model

In the case of this study, the first three Juno orbits are analysed which take place in the dawn sector, near 0600 local time. For reference, 1200 local time is "in front" of the planet and always facing the sun, and midnight local time is on the opposite side of the planet, never facing the sun. This positioning of Juno's initial orbits means that the aforementioned standoff distances do not apply here and must be determined for the

dawn sector. In Figure 2, this has been done using the Joy model (see section 3.4) (Joy et al., 2002). The Juno spacecraft has an apojove of approximately 112 Jupiter radii. In the context of the Jovian magnetosphere boundaries, this means that the spacecraft will likely cross the magnetopause many times during its orbit, (provided it is not extremely rarefied), but will likely not cross the bow shock unless it is compressed by the solar wind. This is clearly shown in Figure 2 as the Juno trajectory (black line) does not cross the bow shock at the observed median location (blue line) determined in the Joy et al. study.

2.2.2 Io torus and the Plasmashell

Of Jupiter's four largest moons, Io, Ganymede, Europa and Callisto, Io is the only volcanically active satellite. A paper published by Peale et al. (1979), concludes that the dissipation of tidal energy induced by Jupiter on Io has caused a significant proportion of the moon to melt. As a result, the moon is covered with many active volcanoes. This

has an implication for the Jovian magnetosphere as the moon is ejecting approximately a tonne of plasma into the magnetosphere every second. As mentioned before, Jupiter has a rotation period of approximately 10 hours, this is close to four times faster than the orbital period of Io (which is approximately 42 hours). This difference in period leads to the production of the plasma torus along Io's orbital path, aptly named the Io torus. The magnetic field of Jupiter causes the Io torus to corotate with the planet. The plasma in the torus is transported outward by inertial force to form the plasmasheet on the night side of the planet where there is little pressure from the solar wind (Louis, C., 2021).

2.2.3 Coordinate Systems

For the purposes of this study, in the case where figures displaying the Juno trajectory or magnetopause and bow shock locations are included, the Jupiter-Solar coordinate system (JSO) is used instead of the planetocentric system.

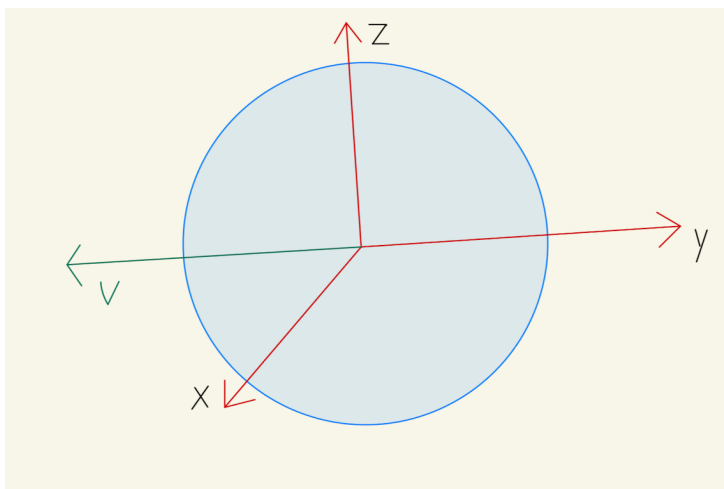


Figure 3: The JSO coordinate system. In this case the X axis is orientated in the sunward direction, the Y axis in the direction of the suns motion from the Jupiter frame and the Z axis completes the orthogonal system ($X \times Y$)

In the JSO system, the X-axis is always pointed in the sunward direction and the Y-axis is orientated in the direction of the suns motion in the Jupiter reference frame. The Z-axis in this case is given by $X \times Y$ as opposed to being aligned with the Jupiter spin axis (as is the case in the planetocentric coordinate system). In the planetocentric case, the X-axis corresponds to the the point of

0° latitude and 0° longitude (prime meridian). By this definition, the planetocentric coordinate system rotates with Jupiter. As a result of this, it proved more suitable to use the JSO coordinate system for this study, as it is fixed in the solar system frame.

2.3 Jovian Radio Emission

Jovian radio emission has long been observed by radio telescopes on the surface of the Earth. However, due to the Earth's ionosphere, which prevents emission below 10 MHz, only radio emissions in the decametric range are detectable. Thanks to missions such as Voyager 1 and 2, Cassini, and now Juno, Jovian radio emissions at lower frequencies can be observed.

2.3.1 The Components of the Jovian Radio Emission

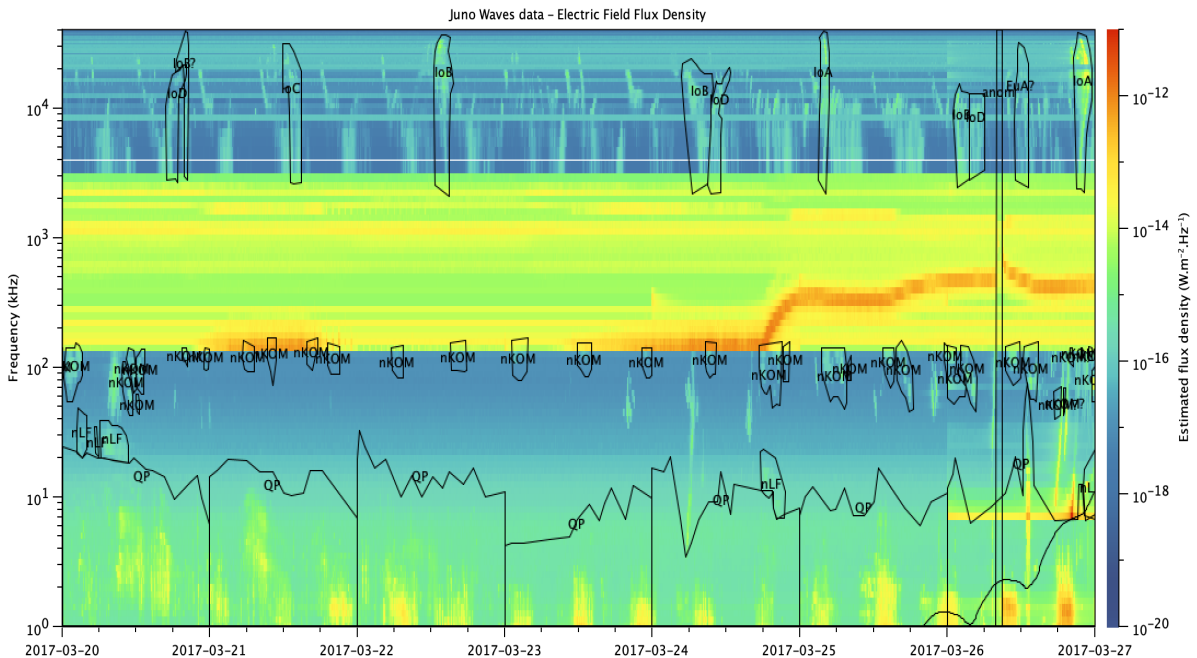


Figure 4: A dynamic spectrum with the components of the Jovian radio emission labelled from the Louis et al. catalogue 2021b. Note here that the bKom emission is the unlabelled kilometric emission.

The known components of the Jovian emission include the aforementioned decametric emission (DAM), broadband kilometric emission (bKom), narrowband kilometric emission (nKom), narrow-band low frequency emission (nLF) and quasi-periodic emission (QP). These emissions are labelled in the dynamic spectrum in Figure 4. A part of the DAM emission is induced through the interaction between Io and Jupiter, thus on many of the time/frequency maps (known as Dynamic spectra) the DAM emission is labelled as Io and non-Io. The DAM emission source is in the auroral region and is emitted through cyclotron maser instability (CMI), the conditions for which are that there is a high magnetized depleted plasma; meaning that the magnetic field is much stronger than the plasma density (Louis, C., 2021). The DAM emissions typically range from 1 MHz

up to approximately 40 MHz. Io DAM is not thought to be influenced by the contraction of the magnetosphere. However, a paper published by Hess et al. (2012), found that the non-Io DAM emission varies only with periods of large magnetospheric compression .

In a similar sense, Louran et al. (1998), found that nKom and bKom also vary during periods of compression. The source of the bKom emission is also in the auroral regions of Jupiter and the emission mechanism for bKom is also CMI. On the dynamic spectrum, the bKom emissions stretch over a large range of frequencies and have a spectral range from a few kHz up to a few hundreds of kHz.

The focus of this study is nKom. In contrast to DAM and bKom, the source for nKom emission is believed to be located in the Io plasma torus and the plasma sheet. It is not currently known for certain what the emission mechanism of nKom is, however it is suspected to be emission close to the plasma frequency and thus may be directly linked to the density of the plasma torus. On the dynamic spectrum, and as the name suggests, nKom appears narrow in relation to the frequency axis, typically spanning only a few tens of kHz. nLf emission is also thought to vary with magnetospheric compression although more investigation is needed to confirm this. The emission process for nLF is unknown but thought to be the same as nKom, however occurring at different source locations. nLf emissions appear very similar to nKom emission but occur at lower frequencies typically up to a few tens of kHz.

Finally, QP emission is a repetitive pulse of emission with a quasi period of approximately fifteen or forty minutes. QP has a spectral range of 1Khz up to a few tens of Khz. The source of QP emission is above the poles of Jupiter and at high latitudes. The emission mechanism is not currently known, however, it is likely the electron cyclotron frequency (Louis, C., 2021).

3 Computational Method

The majority of the computational work performed to complete this study involved the use of python and python packages such as Numpy, Scipy and Matplotlib to infer results from the Juno telemetry which was obtained in the form of .csv files. As well as python, a data visualisation tool called autoplot was used to create the dynamic spectra from the data that was acquired by the Juno waves instrument. The code that was written for this project can be found at: <https://github.com/Elliott-DH/Senior-Soph-Project/blob/main/SS%20Project%20Code.ipynb>

3.1 Identifying Boundary Crossings

Using the data recorded by the magnetometer on board Juno, it was possible to create a plot of the variance of the magnetic field magnitude with time for the Juno approach and the first three Juno orbits. An example of this is presented in Figure 5, for a two day period during the first Juno orbit after JOI.

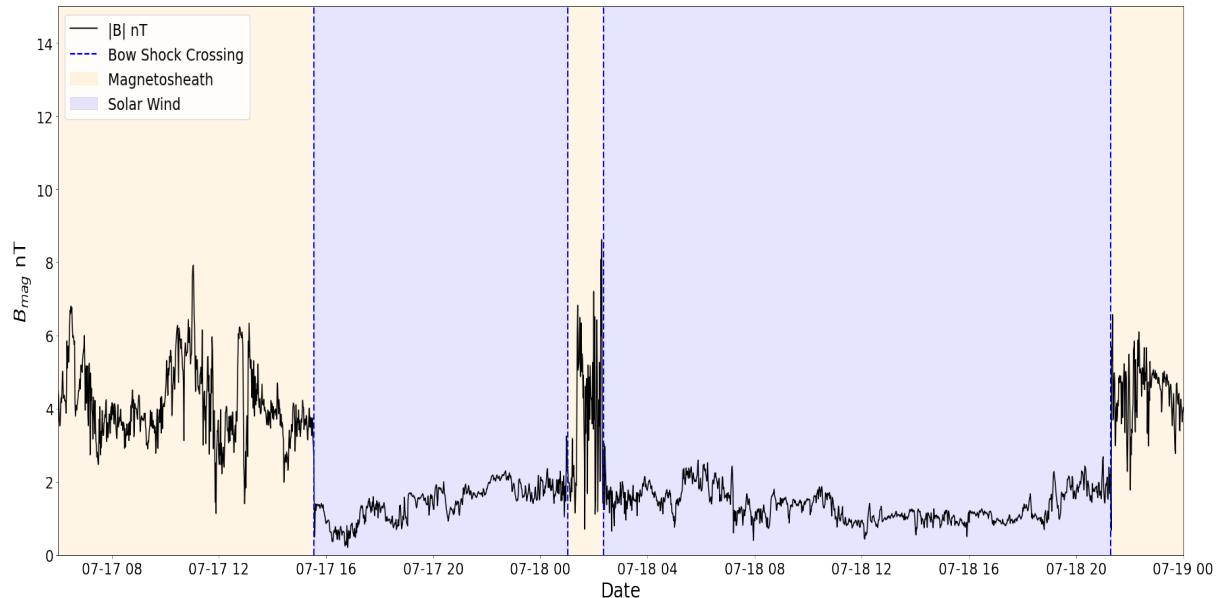


Figure 5: The magnitude of the Jovian magnetic field (black line) from 17/07 (DOY 199) until the end of 18/07 (DOY 200). Here the magnetic field magnitude has been used to determine the region at which the spacecraft crosses the bow shock boundary (blue dashed lines).

Using this figure it is possible to obtain a time for which the Juno spacecraft crosses a magnetospheric boundary. For instance, in the above example the first region the spacecraft is in the magnetosheath as there is a clear instability in the field magnitude as the plasma encountered the bow shock and is now in the turbulent magnetic field.

After this on DOY 199 at approximately 15:30, the spacecraft crosses the bow shock on an outbound crossing into the solar wind. Here the field magnitude is relatively stable in comparison to when it is in the sheath as the solar wind has not yet encountered the bow shock (Jackman, Thomsen and Dougherty, 2019). Another example of this can be seen in section 7 Appendix A. In this case the spacecraft is in the magnetosphere in the first case and crosses into the turbulent magnetosheath. The field magnitude signature of the magnetosphere is harder to differentiate from the magnetosheath, however, it typically is at a higher value and fluctuates less.

It should be noted that for the purposes of this study, due to the time constraint, the boundary crossings identified have been taken from the work of Hospodarsky et al. (2017); which used the above method and others to determine the time and location of the boundary crossings for Juno's approach to Jupiter and for the first three orbits after JOI.

3.1.1 Juno's Orbital Path

The position of the Juno spacecraft is given in five minute intervals by a set of JSO coordinates. Using this data, it was possible to plot the orbital path of Juno during its approach and three subsequent orbits in the XY plane.

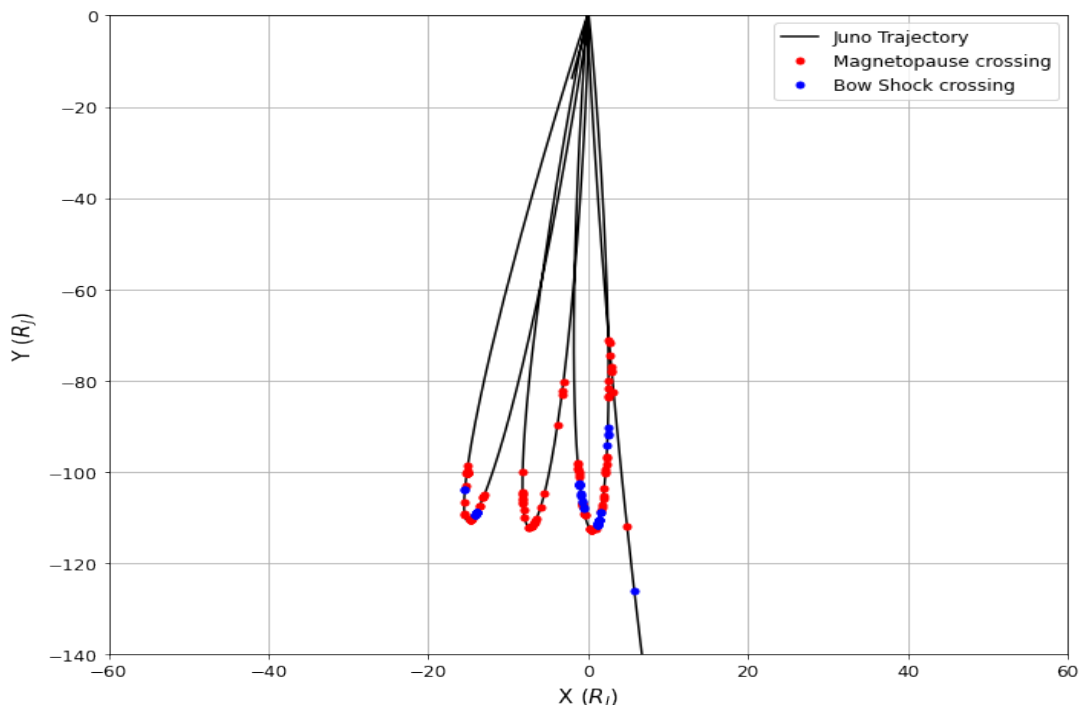


Figure 6: The orbital path of the Juno spacecraft for its approach to Jupiter and its first three orbits in the XY plane(black line). Plotted onto this is the position the spacecraft crossed the magnetopause (red dots) and the bow shock (blue dots) boundaries.

Using the boundary crossing time determined by Hospodarsy et al. (2017) the position of the spacecraft at each of these crossing times could be established. Plotting the crossing positions onto the Juno orbital path in the XY plane allowed for the creation of a visual tool. This can be seen in Figure 6. Similarly, the same plot was created in the XZ and also in a three dimensional space. Both of which can be seen in section 7 in appendix B and D respectively. Furthermore, using the data from Figure 6, a plot demonstrating what region of the magnetosphere the spacecraft is in at each point on its orbit can be generated. This plot is shown in Figure 7.

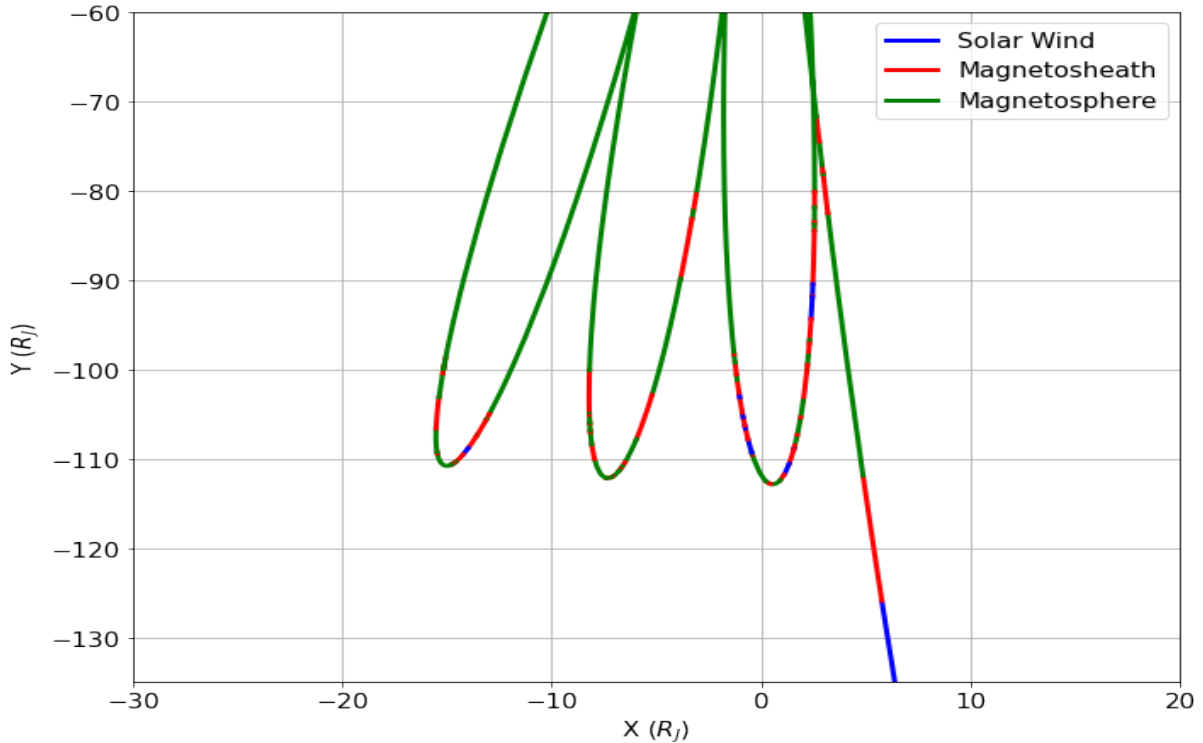


Figure 7: The Juno orbital path, colour coded according to the region of the magnetosphere the spacecraft was in at that point. Here blue refers to the spacecraft being situated in the solar wind, red the magnetosheath and green the magnetosphere.

These figures were created to be used as a tool in the identification of periods of magnetospheric compression. For instance, in Figure 6 (and Figure 7), after the spacecraft has completed JOI and is on its first orbit of Jupiter, it can be seen that the spacecraft crosses the magnetopause and then the bow shock closer to the surface of the planet than expected. This indicates that during this time, the magnetosphere was being compressed by the solar wind and this may be a good period to investigate the behaviour of the nKom emission.

3.2 Autoplot - Dynamic Spectra

The radio wave emission data collected by the Juno-Waves instrument was visualised using the Autoplot application (Faden, Weigel, Merka and Friedel, 2010). The Juno data was stored in a .vap file which was opened within Autoplot. When opened, the data was displayed in the form of a time/frequency map called a "dynamic spectrum", an example of which is shown below in Figure 8. The data used in these plots are from the dataset processed by Louis et al. (2021a).

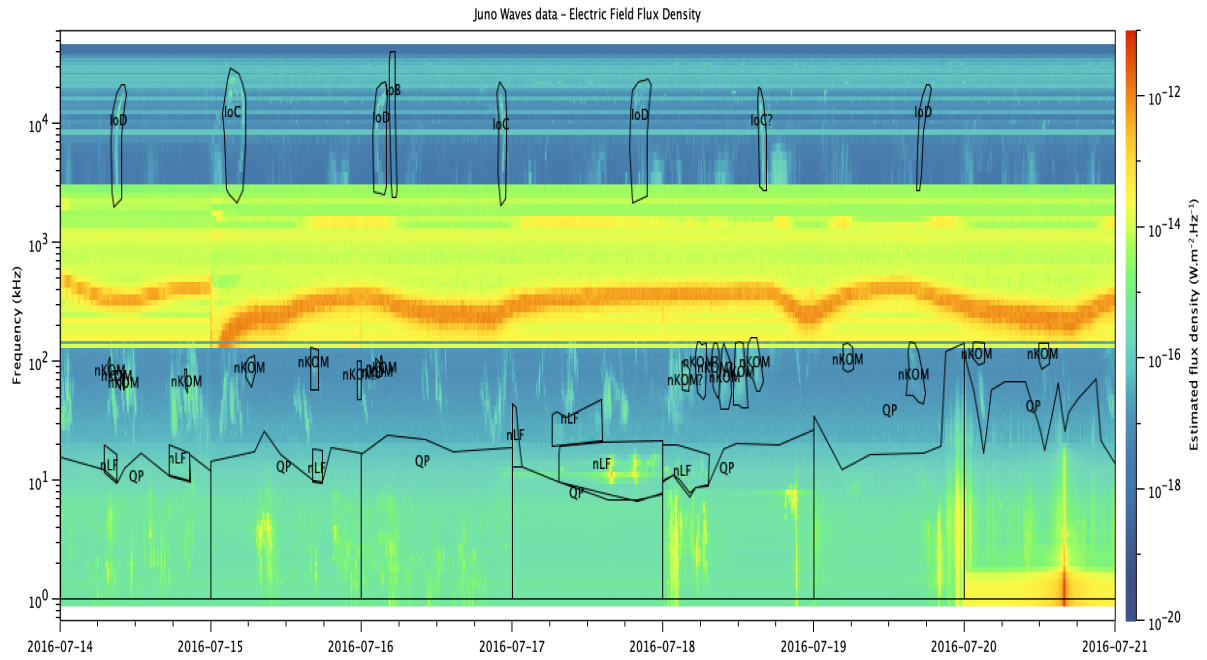


Figure 8: Dynamic Spectrum for DOY 196 through 202

On the Y axis of the dynamic spectrum is the frequency of the radio waves on a logarithmic scale and on the x axis is time. The flux density of the emission is described by a colour map which ranges from $10^{-20}W \cdot m^{-2} \cdot Hz^{-1}$ to $10^{-12}W \cdot m^{-2} \cdot Hz^{-1}$. The labelling of emissions on all of the spectra in this study is from the Louis et al. catalogue, 2021b. It should be noted here that due to an error with the waves instrument, there is a band of interference in the hectometric range and in the low decametric range. Unfortunately, this is consistent throughout the entire spectrum and thus appears in all of the spectra presented in this study.

3.3 nKom Time series

In addition to the dynamic spectra, nKom emissions can also be displayed using time series files which were also created using the “Catalogue of Jupiter radio emissions identified in the Juno/Waves observations” (Louis et al. 2021b). The time series data are stored in .sav files. Using the readsav command from the Scipy package, these files are read into Python. The data in these files allows for the display of the variation in time of the intensity of specific frequencies of radio emission.

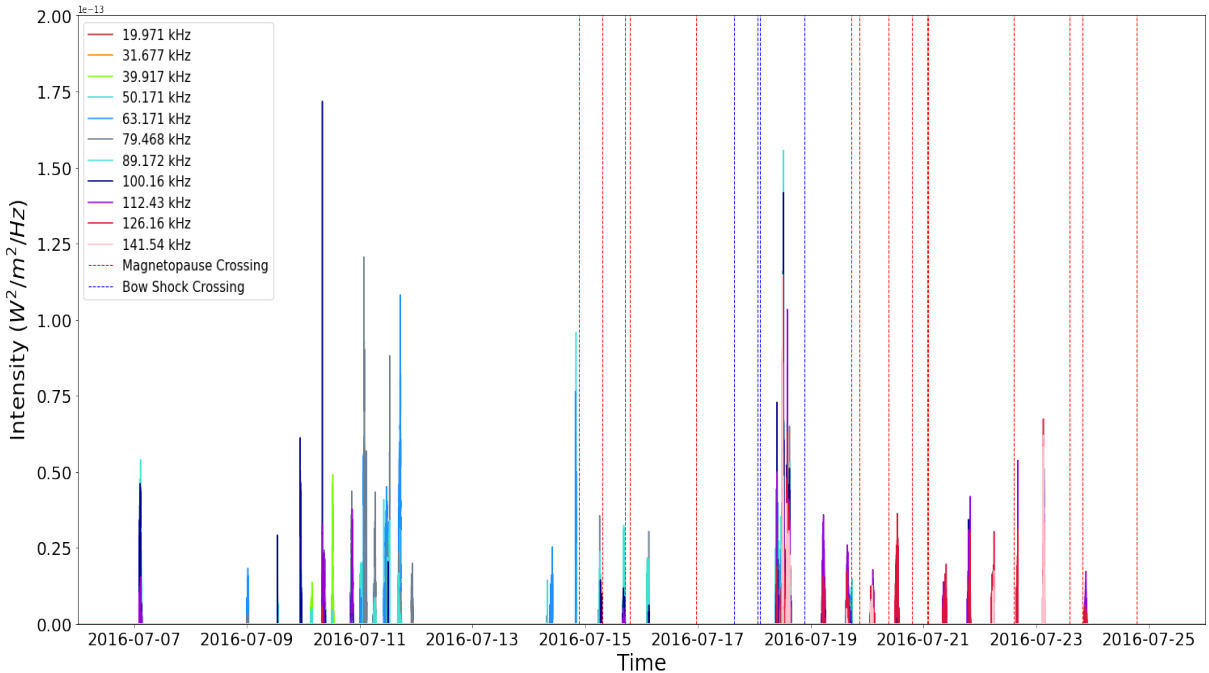


Figure 9: Time series for 6 specific frequencies 19.971 kHz, 39.917 kHz, 63.171 kHz, 89.172 kHz, 112.43 kHz, 141.54 kHz for the period from DOY 188 to DOY 208. The blue and red lines here represent the time at which Juno crossed the magnetopause and bow shock respectively.

When used in conjunction with the dynamic spectra, the nKOM time series figures allow for an accurate measurement of certain characteristics of the emission such as the period between bursts and is a useful mechanism for determining information about the emission during periods of magnetospheric compression. In the time series figures presented in this study, only frequency bands as high as 140 kHz have been included due to the issue regarding the Waves instrument. Frequency bands above 140 kHz cannot be visualised on dynamic spectra and thus have been excluded from the time series plots.

3.4 The Joy et al. Model

The Joy et al. model is a model of the Jovian magnetopause and bow shock boundary surfaces. For the purposes of this study, the Joy et al. (2002) model will predict the location of the two boundaries given a value of solar wind dynamic pressure. In addition to this, given a set of X,Y,Z coordinates of a boundary crossing location, the model will return the dynamic pressure associated with the boundary surface being located at these crossing coordinates. The model uses data from a number of spacecraft that have encountered Jupiter's magnetosphere including: Pioneer 10 and 11, Voyager 1 and 2, Ulysses and Galileo. In this model, the shapes and position of the boundaries are influenced by the solar wind dynamic pressure via a simulation called the Ogino-Walker magnetohydrodynamic simulation and through observations of the spacecraft listed above (Ogino, Walker and Kivelson, 1998), (Joy et al., 2002). The shape of the surfaces are determined by a collection of points lying on the surface. These points are given as least square fits to a second order polynomial given below:

$$z^2 = A + Bx + Cx^2 + Dy + Ey^2 + Fxy \quad (5)$$

(Joy et al., 2002). In order to reduce error in the least square fit, the lengths are scaled by a factor of 120. The boundaries are fitted for four values of dynamic pressure: 0.045 nPa, 0.090 nPa, 0.180 nPa and 0.360 nPa, to the polynomial given in equation (5). The coefficients of the polynomial are then fitted to power law models of dynamic pressure which results in a function that will return boundaries as a function of dynamic pressure. This is given below in equation 6:

$$Z^2 = A(P_{dyn}) + B(P_{dyn})x + C(P_{dyn})x^2 + D(P_{dyn})y + E(P_{dyn})y^2 + F(P_{dyn})xy \quad (6)$$

From analysis of spacecraft observations, the probability of the magnetopause and bow shock surfaces existing in different locations can be determined. Using these probabilities, the values of dynamic pressure that correspond to a compressed or rarefied surface are established. Joy et al. (2002) found that a compressed magnetopause had an associated dynamic pressure value of 0.306 (+0.108, -0.078) nPa. Additionally, it was determined

that the dynamic pressure value corresponding to a compressed bow shock location was 0.315 (+0.148, -0.104) nPa. This will be the criteria that will ascertain whether or not the magnetopause/bow shock is compressed or not in this study. For instance, if Juno crosses the magnetopause at a certain location, the X,Y,Z coordinates of this location will return a value of solar wind dynamic pressure using the Joy et al. model. If the returned value of dynamic pressure falls into or exceeds that of the values given in the Joy et al. (2002) paper for a compressed magnetopause, it can be deemed that the magnetopause surface that Juno encountered is in a compressed state.

3.4.1 Using the Joy et al. Model for Boundary Crossings

Using the Joy et al. model, two functions are defined. One function will return a surface given a value of dynamic pressure (one for magnetopause and one for bow shock) and the other function will return a dynamic pressure value given a X,Y,Z coordinate. An example of the first function is displayed in section 7 appendix C. Here, a range of dynamic pressure values have been input into the Joy et al. model, and the surfaces that each value returns has been plotted onto Juno's orbital path. These figures allow for simple identification of the locations where Juno encountered a boundary during a period when that boundary was compressed.

For example, early on Juno's second orbit, it can be seen that the spacecraft encounters the magnetopause four times near the surface, corresponding to a dynamic pressure of 0.35 nPa. If it is now assumed that this is a period of magnetospheric compression, the X,Y,Z coordinates of Juno at these crossing times can be input into the second function that has been defined in order to return the exact values of the dynamic pressure for each of these crossings. Unfortunately, the function will only return a value given the X,Y,Z coordinates of a magnetopause crossing and will not return a value for a bow shock crossing. As a result, the dynamic pressure of the bow shock crossing events has been determined by using plots similar to that shown in appendix C, and inputting values of dynamic pressure until the equivalent bow shock surface crosses the location in which Juno encountered the bow shock. As this method of determining the dynamic pressure value for each bow shock crossing is less accurate than using the model, dynamic pressure values for the magnetopause crossings are primarily used as compression indicators in this study.

4 Results and Discussion

4.1 Statistical Analysis of Boundary Crossings

All of the boundary crossings that occurred during Juno's approach and first three orbits of Jupiter have been identified, attached to each is a value for time, distance from Jupiter's surface, and dynamic pressure. It is now possible to conduct statistical analysis on the crossing data. This has been done in terms of distance and dynamic pressure.

4.1.1 Distance from Jupiter's Surface

Here, the boundary crossings have been represented by the distance at which Juno crosses the boundary from Jupiter's surface. Each distance is given in terms of Jupiter radii (R_J).

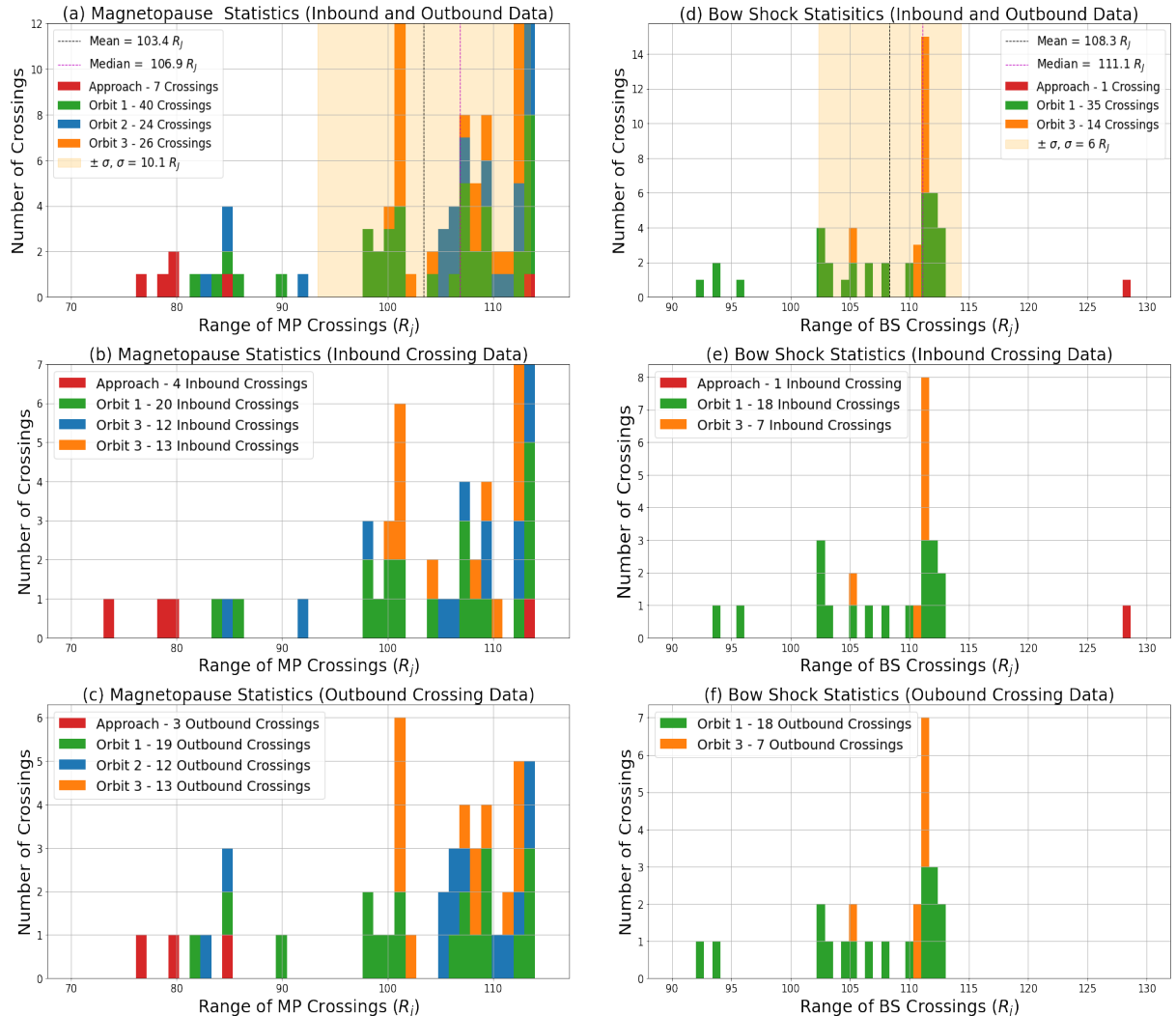


Figure 10: Histograms detailing how many boundary crossings occurred at a certain distance from the surface of Jupiter. The three histograms on the left display the magnetopause crossings with (a) containing inbound and outbound crossings, (b) inbound crossings and (c) outbound crossings. The three histograms to the right display the same data but for the bow shock encounters.

In Figure 10, the magnetopause and bow shock crossings have been sorted (colour) by the orbit on which it occurred. In addition to this, two further histograms (b,c and e,f) distinguish as to whether the boundary crossing was an inbound crossing or an outbound crossing. For example, an inbound crossing indicates that the spacecraft crossed the magnetopause, going from the magnetosheath to the magnetosphere, whereas an outbound crossing indicates a magnetopause crossing from magnetosphere to magnetosheath. The same applies to the bow shock crossings in terms of magnetosheath and solar wind.

In Figure 10, the mean distance of a magnetopause crossing is determined to be $103.4R_J$, while the median value is $106.9R_J$. The standard deviation of the magnetopause crossing data is $10.1R_J$. For the bow shock boundary crossings, the mean value is $108.3R_J$, while the median value is $111.1R_J$. The standard deviation of the bow shock boundary crossings is smaller than that of the magnetopause, at $6R_J$. As mentioned in section 2.1.1, the nature of Juno's orbital path means that it will likely not cross the bow shock unless the magnetosphere is under a period of compression from the solar wind. This should be taken into consideration when analysing the bow shock crossing data presented in Figure 10. Excluding the crossing on Juno's approach at a distance of $128.1 R_J$, it is likely that all of the other bow shock crossings occur as a result of magnetospheric compression, the strongest of which can be identified on histogram (d), in the four crossings at the very left of the histogram in the region of $90R_J$ to $96R_J$.

4.1.2 Dynamic Pressure

As described in section 3.4, using the Joy et al. model, a value for the dynamic pressure has been associated with each boundary crossing. This value corresponds to the dynamic pressure that would cause the magnetopause or bow shock to be located at the point that Juno encountered it. In Figure 11, two histograms displaying the number of crossings at a certain value of dynamic pressure are included, (a) displays the magnetopause crossings and (b) the bow shock crossings. The mean dynamic pressure value for the magnetopause crossings is 0.214 nPa, the median is 0.204 nPa, and the standard deviation is 0.027 nPa. For the bow shock encounters, the mean is 0.471 nPa, the median is 0.468 nPa and the standard deviation is 0.095 nPa. Also included in Figure 12, is a comparison of the median values of dynamic pressure for magnetopause and bow shock crossings determined from this study and the observed median values given in the Joy et al. (2002) paper.

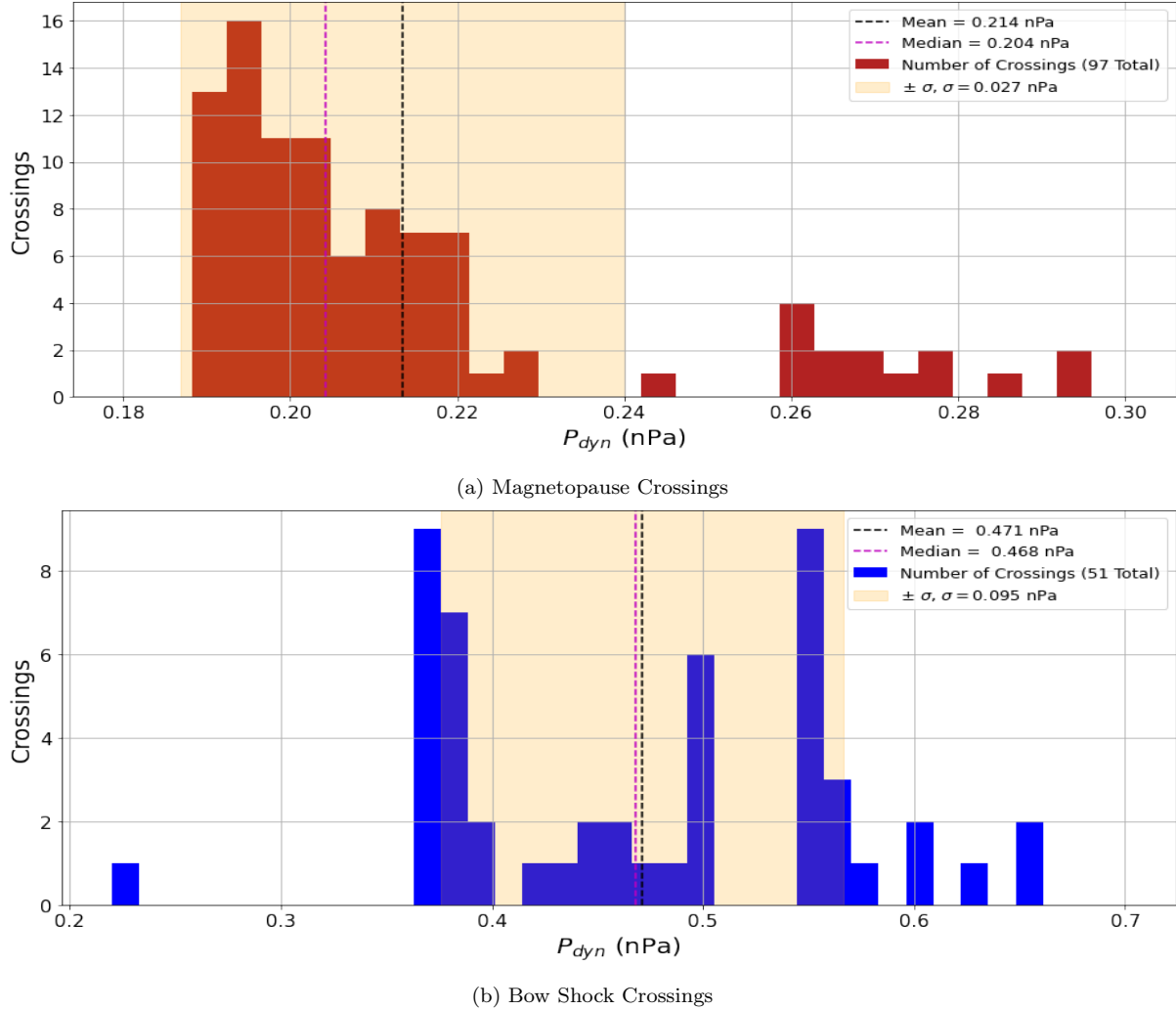


Figure 11: Histograms displaying the range of dynamic pressure values corresponding to each magnetopause crossing (top) and bow shock crossing (bottom).)

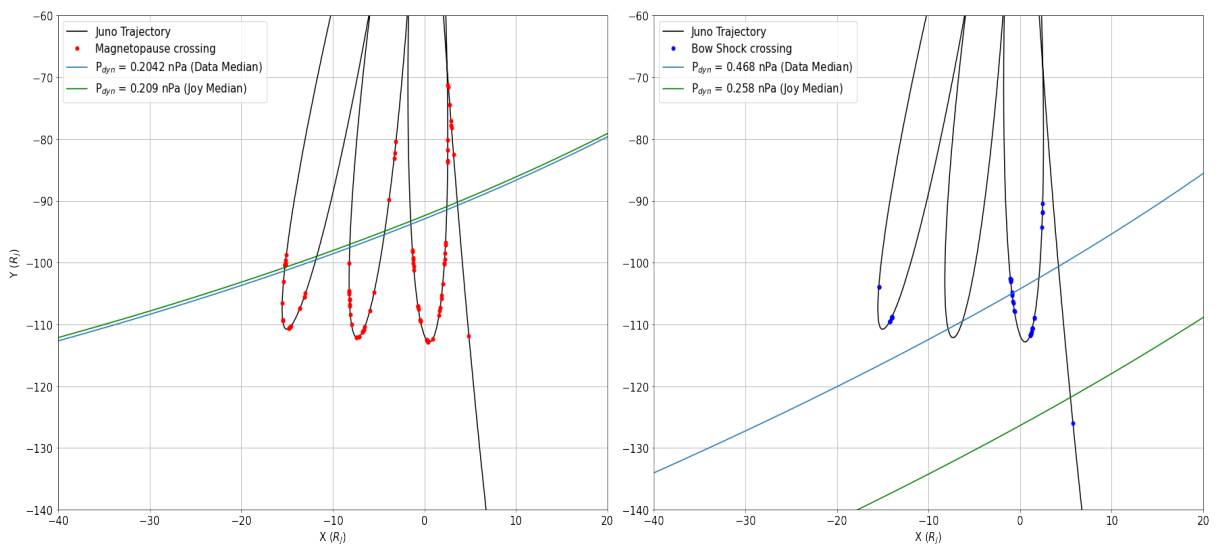


Figure 12: Left: A comparison between the magnetopause boundaries produced by the median dynamic pressure from this study (blue) and that from the Joy et al. study (green). On the right is the same plot but for the bow shock medians (Joy et al. (2002))

As can be seen in Figure 12, there is agreement between the two median values of dynamic pressure for the magnetopause crossings. However, there is a difference of 0.21 nPa between the bow shock median values. The median value from the Joy et al. (2002) paper uses data from numerous spacecraft to determine the observed median position of the bow shock. The discrepancy between the two values arises from the issue regarding Juno's apojoove distance not being sufficiently far from Jupiter to encounter the bow shock in a relaxed state. Therefore, while in this study the bow shock has been observed in a compressed state, the observed median from the Joy et al. (2002) is more accurate as it included data from when the bow shock is in relaxed and rarefied states also.

4.2 Determination of Magnetospheric Compression Periods

The first period of magnetospheric compression identified in this study occurred on DOY 180 and DOY 181 during Juno's approach to Jupiter. The spacecraft was in the magnetosphere and encountered the magnetopause on an outbound crossing to enter the magnetosheath late on DOY 180 at a distance of $84.4R_J$. It then crossed the magnetopause a further five times, the last of which occurring close to midnight on DOY 181 at a distance of $73.5R_J$. Using the Joy et al. model the position of the magnetopause on this final crossing represents a corresponding dynamic pressure of 0.29 nPa. This falls within the range of dynamic pressure values that indicate a compressed magnetosphere as determined by Joy et al. (2002), (see section 2.2.2).

The second period of compression that has been identified was indicated by an outbound magnetopause crossing on DOY 196 (early on Juno's first orbit with distance from Jupiter increasing in this stage), at a distance of $82.0R_J$. The corresponding value of dynamic pressure for this location is 0.270 nPa. Thus, it can be inferred that this is also a period of compression. The spacecraft crossed the magnetopause four times on DOY 197 and 198 at distances further from the planet until crossing the bow shock outbound into the solar wind on DOY 199 at a distance of $92.1R_J$. The bow shock being this close to Jupiter is a good indication of compression and the dynamic pressure of a bow shock surface at this distance is 0.633 nPa. However this value is likely inaccurate due to the aforementioned error with the Joy function and the nature of the fitting process. For this reason, while the location of the bow shock is still a good indicator of compression, only the dynamic pressure of magnetopause crossings will be used in the determination of

magnetospheric compression. Another period of compression was identified during Juno's second orbit on DOY 250. The spacecraft crossed the magnetosphere on an outbound crossing at a distance of $82.6R_J$, corresponding to a dynamic pressure value of 0.267 nPa. Finally, the last time the spacecraft encountered the magnetopause on its second orbit took place on DOY 278 at a distance of $98R_J$. While this is further from Jupiter than previous values, due to the second orbit being later in the dawn sector than the first, and due to the nature of the flank of the magnetosphere boundary, (see Figure 12), this crossing corresponds to a reasonably high value of dynamic pressure at 0.215 nPa. Figure 13 displays all of the boundary crossings that indicate compression mentioned above.

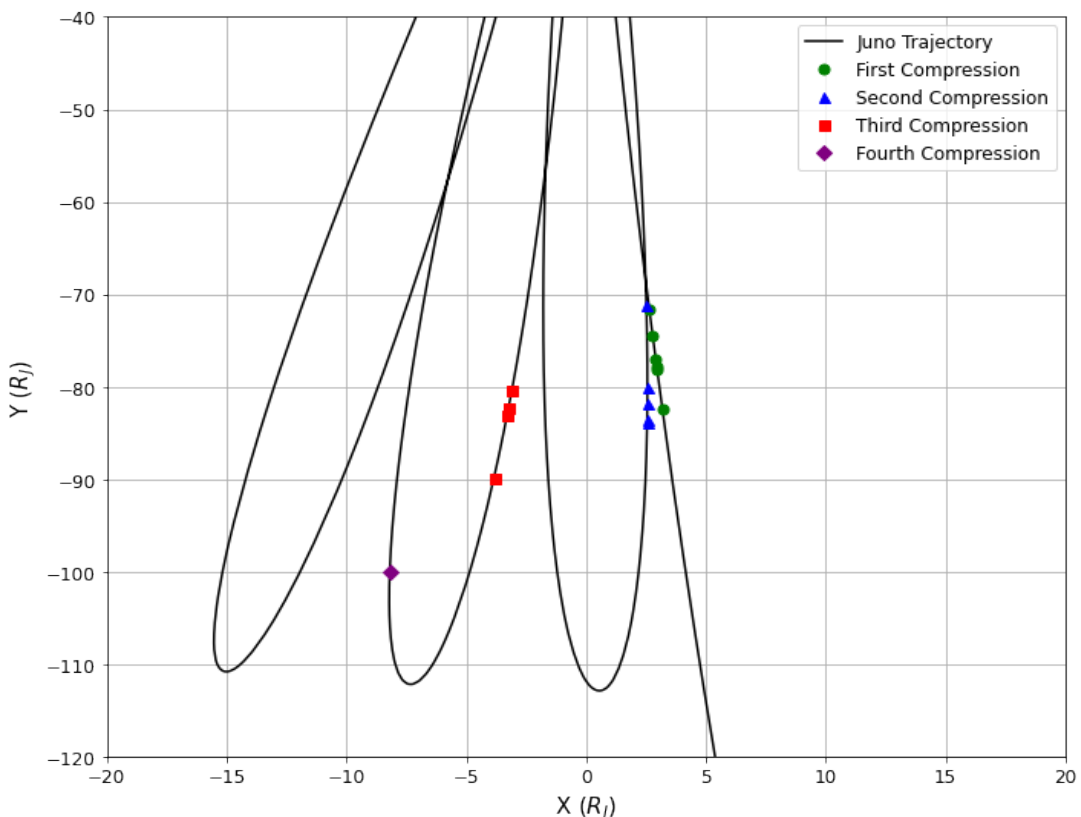


Figure 13: The Juno Trajectory with the magneto pause crossings that represent the first (green), second (blue) third (red) and fourth (purple) magnetospheric compression periods.

4.3 nKom Emission During Magnetospheric Compression

As four periods of magnetospheric compression have been identified, the nKom emission before, during and after each of these periods can now be analysed for signs of increased intensity and periodicity. Unfortunately, from approximately DOY 182 until DOY 188, the Juno-Waves instrument was not operating as the spacecraft was being maneuvered for

orbit insertion during this time. As a result, the dynamic spectrum for this period is not fully available and thus, the nKom emission cannot be analysed during this compression. The data that was recorded (before and after the instrument was turned off) is included in appendix E for completeness.

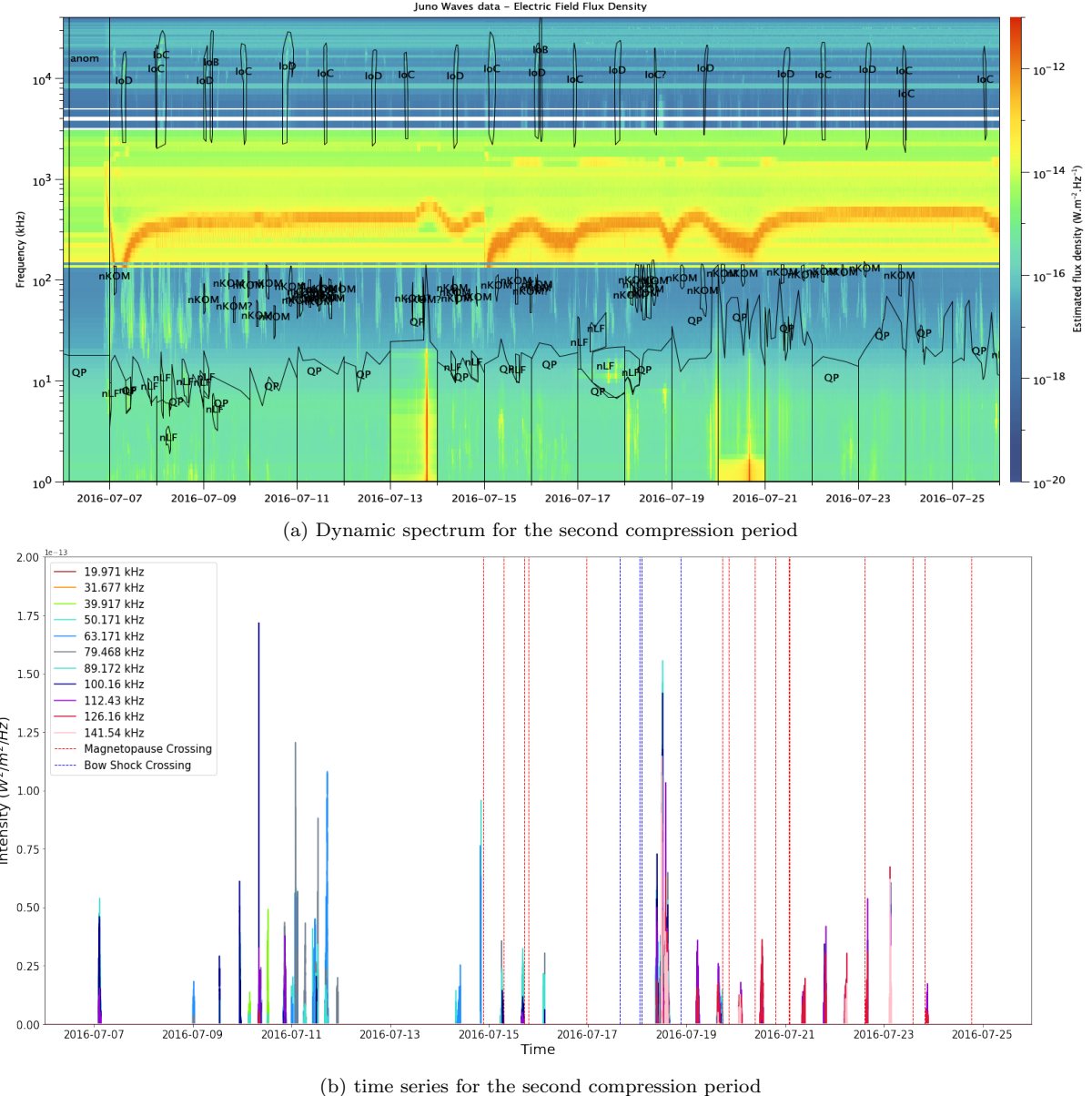


Figure 14: (a) The dynamic spectrum (top) and time series (bottom) for the second magnetospheric compression identified (DOY 188 - 207). In the dynamic spectrum, the instances of nKom emission have been labelled (Louis et al. catalogue, 2021b.). In the time series, the magnetopause and bow shock crossings are indicated by the red hatched lines.

The dynamic spectrum and time series for the second period of magnetospheric compression are displayed in Figure 14. As previously mentioned, during this compression, Juno first crossed the magnetopause late on DOY 196. The spectrum and time series in Figure 14 begin on DOY 188, as it was noticed that there was significant nKom emission

before DOY 196. This likely means that the compression of the magnetosphere began before Juno first encountered the magnetopause.

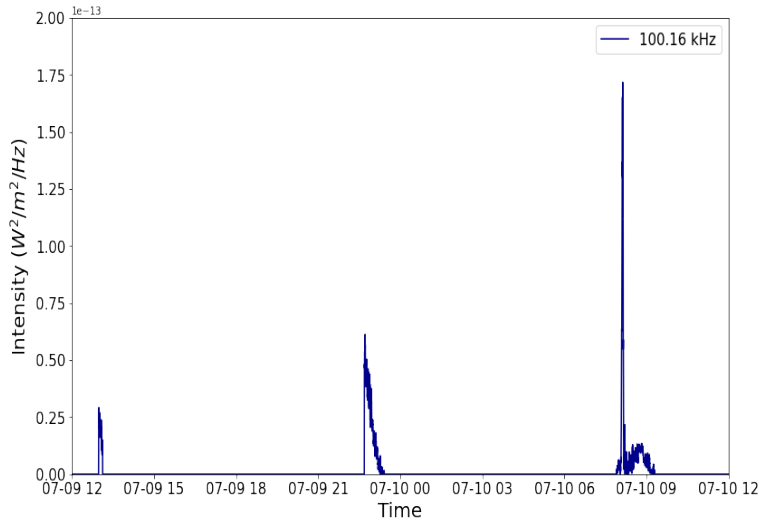


Figure 15: Timseries of the 100.16 kHz frequency band over the course of DOY 190.

that there is approximately a 10 hour period between emission and an increase in the intensity of the emission over time. Similar patterns are observed with the 63.171 kHz and 89.172 kHz frequency bands, however, these bands do not exhibit the same intensity as the 100.16 kHz band.

The next burst of emission occurs approximately two days after the first, beginning late on 14/07 (DOY 194) and lasting until late on 15/07 (DOY 195). This emission burst can be seen in appendix F. During this period, the 63.171 kHz frequency band is the most intense. It also displays an approximately ten hour periodicity. The second observed emission of this frequency band is more intense than the first, however, the two subsequent emissions are less intense. Also during this second burst, a lone emission of the 50.171 kHz band is detected at the same time as the second emission of the 63.171 kHz band and at the same intensity. For the 50.171 kHz band however, there were no subsequent emissions and hence no indication that it was periodic. A more precise time series figure for this burst is included in appendix F.

The final burst of nKom emission during this compression occurs on 18/07 (DOY 198) and continues until 24/07 (DOY 204). Figure 16 shows four different frequency bands during this burst, 100.16 kHz, 112.43 kHz, 126.16 kHz and 141.54 kHz.

From looking at Figure 14, it is immediately clear that there is more active nKom emission during this time. Examining the first burst of emission from 09/07 (DOY 190) until approximately 12/07 (DOY 193), and isolating the 100.16 kHz frequency band shows that there is periodicity in the emission. Figure 15 shows

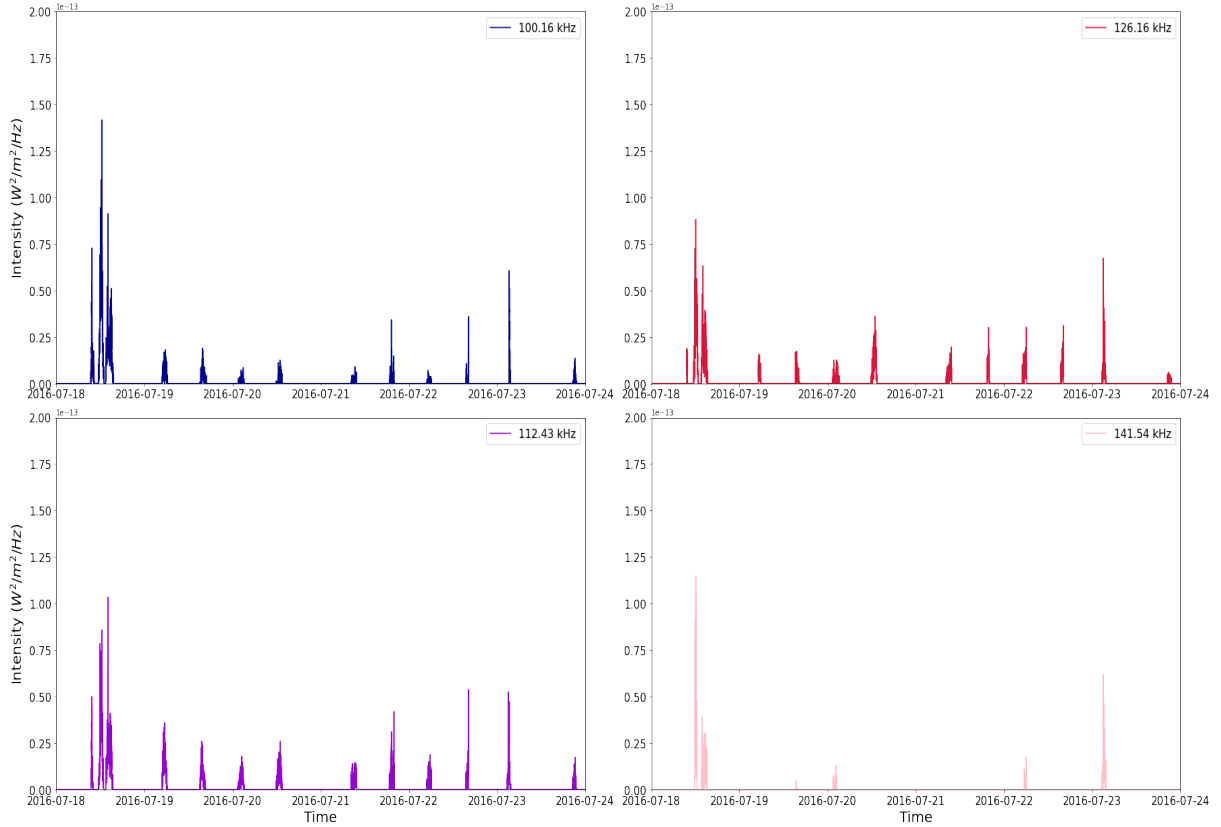


Figure 16: The behaviour of the 100.16 kHz (blue), 112.43 kHz (purple), 126.16 kHz (red) and 141.54 kHz (pink) frequency bands during the third burst of emission during this compression.

Here, the 100.16 kHz, 112.43 kHz and 126.16 kHz frequency bands all behave in a similar manner. Each begins with three of the most intense emissions during the period, all separated by approximately two hour intervals. After this, there is a delay of around 16 hours between the last of the three initial emissions and the next emission, which is significantly less intense. The next three emissions display the previously observed ten hour periodicity and are all of a similar intensity. There is then another delay, this time of 20 hours before the emissions continue again. There are then five emissions, with resumed ten hour periodicity and having a general trend of increasing intensity. It should be noted that the 141.54 kHz frequency band also begins with an intense emission, however the following emissions are not intense enough to be able to infer if it is displaying the same pattern as the other three frequency bands.

The third period of compression that was identified in this study, was indicated by a magnetopause crossing on DOY 250. The period of which there was notable nKom emission has been taken from 09/05 (DOY 249) until 21/09 (DOY 265). The dynamic spectrum and time series for this period are shown in Figure 17.

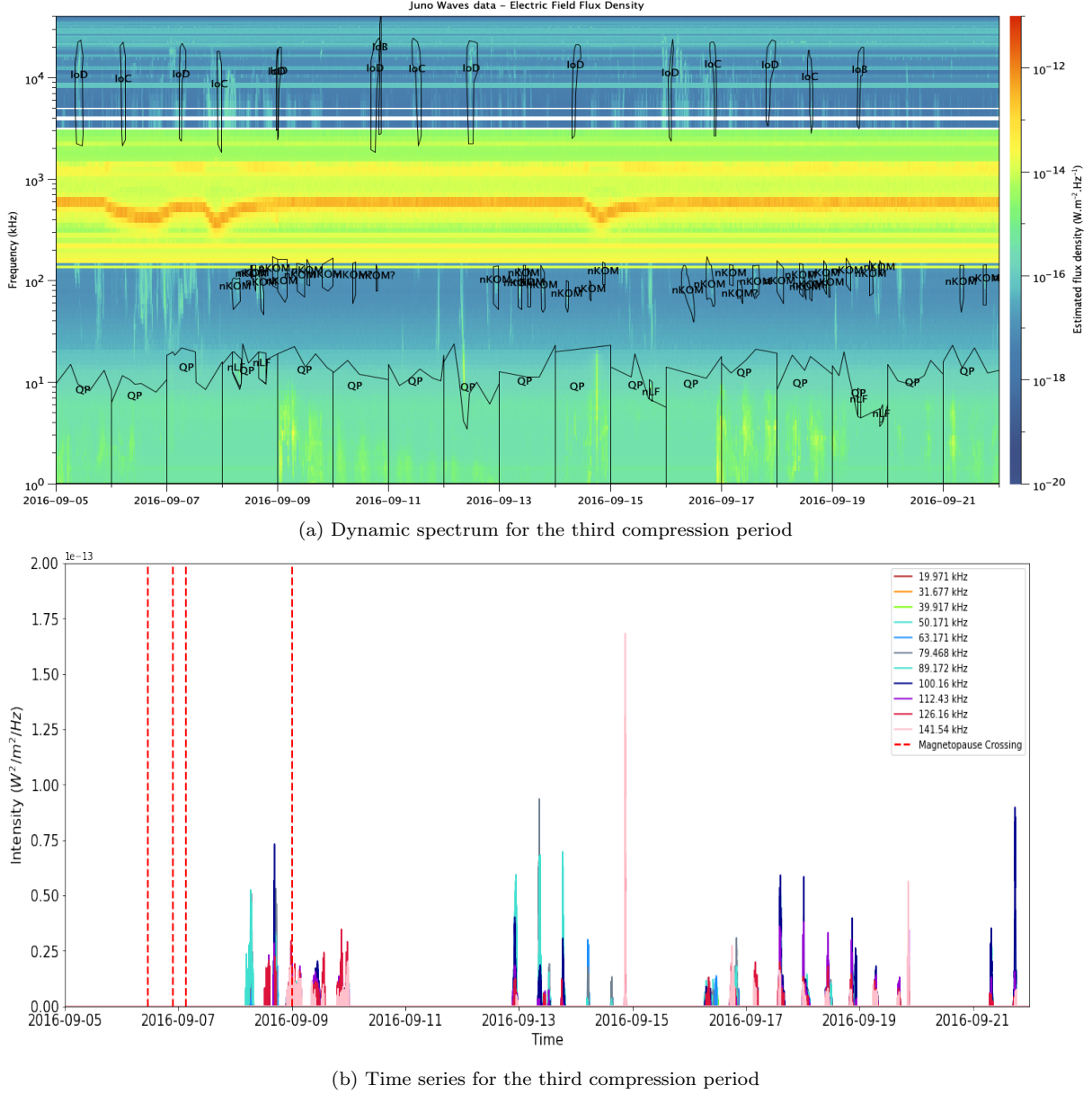


Figure 17: (a) The dynamic spectrum (top) and time series (bottom) for the third magnetospheric compression identified (DOY 249 - 265). Note that only the four magnetopause crossings (red hatched lines) that indicate compression have been included in the time series plot.

In this period, there are also three bursts of emission, the first of which begins on 08/09 (DOY 252) and ends late on 09/09 (DOY 253). A more precise time series for this burst can be seen in appendix G. This burst therefore occurs approximately 2 days after Juno has initially crossed the magnetopause and detected compression. The first emission in this burst is dominated by the 63.171 kHz, 74.468 kHz and 89.172 kHz frequency bands, the second emission (which occurs 10 hours later), also contains these frequency bands as well, but also an intense emission of the 100.16 kHz band. There are three subsequent emission events after this. They are mostly composed of higher frequency bands, 100.16 kHz, 112.43 kHz and 126.16 kHz and 41.54 kHz, and are less intense than the initial two.

Interestingly, while they are not as intense, they appear to last longer with each emission lasting approximately 6 hours.

The second burst during this compression began late on 12/09 (DOY 256) and ended on 14/09 (DOY 258). The first three emissions are again separated by ten hour intervals and consist mainly of the 79.468 kHz, 89.172 and 100.16 kHz frequency bands. After these three emissions there is another emission ten hours later that shifts to 63.171 kHz and 79.468 kHz and is much less intense. This is followed ten hours later by an emission which is less intense again. Finally, six hours after this, there is an emission of 126.16 kHz and 141.54 kHz that is much more intense than any of the previous emissions during this burst. The time series for this second burst is shown in appendix I.

The third emission burst during this compression began on 16/09 (DOY 260) and lasted five days ending on 21/09 (DOY 265). The time series for this specific burst can be seen in appendix H. This burst consists of nine emissions, the first beginning at approximately noon DOY 260 and the last near midnight on DOY 263, followed by a delay of approximately 30 hours and then two further emissions separated by ten hours. Starting with the first nine emissions, the trend noticed here is that the emissions grew stronger and then weakened meaning that the fourth and fifth emissions were the most intense. The first two emissions appear to last longer than the following seven, and consist of many frequency bands from 39.917 kHz to 141.54 kHz. The next seven emissions appear to be shorter in duration and composed of higher frequency bands, 100.16 kHz up to the 141.54 kHz bands. The last emission of the nine appears to break the pattern as it begins with weak emission followed by a gap of four hours and then an intense emission (relative to the previous eight) of the 141.54 kHz and 112.43 kHz bands. Following these nine emissions and after the 30 hour gap of no emission, there are two emissions of primarily 89.172 kHz and 100.16 kHz frequency, the second of which is the most intense of the entire burst.

The fourth and final compression identified in this study was indicated by an inbound magnetopause crossing on 4/10 (DOY 278). The nKom emission during this compression was observed from 03/10 (DOY 277) until 12/10 (DOY 298). The dynamic spectrum and time series for this emission period can be found in appendix J. This emission can be divided into two bursts, separated by a gap of approximately twenty hours after the

final emission of the first burst on 09/10 (DOY 295). The first burst lasts for six days and begins with seven emissions with a ten hour period of 79.468 kHz to 100.16 kHz. The general trend of the emission appears to be decreasing with intensity, however the third and fourth emissions are much less intense than the others. After the initial seven emissions, there is a weak eighth emission followed by a strong ninth emission composed of higher frequencies than the previous eight. Ten hours after this there is an emission roughly half as intense as the previous and made up of higher frequencies again (126.16 kHz - 141.54kHz). Interestingly however, these two emissions are separated by a much weaker emission, occurring roughly five hours after the first. This means that the ten hour periodicity of the first eight emissions is no longer present for the final emissions of this burst.

The second and final burst of this period begins 20 hours after the first burst. It starts with a strong emission of 79.468 kHz at approximately 18:00 on 09/10 (DOY 295), and is followed by two weaker emission each separated by ten hours and of higher frequencies. After the third emission, there is a gap of approximately six hours before there is an intense emission of 79.468 kHz again. The final emission of this burst occurs ten hours after the previous and is much less intense.

4.4 Discussion of Results

From observing the nKom emission before, during and after each of the identified compression periods it is clear that there is more active emission during magnetospheric compression. During the second compression there is nKom emission as intense as $1.75 \times 10^{-13} W \cdot m^{-2} \cdot Hz^{-1}$. The ten hour periodicity that was observed in the first burst of nKom emission during this compression, means that the source of the emission is longitudinally fixed. The rotation of Jupiter is approximately 10 hours and therefore, as the source has fixed longitude, the emission is observed as it comes into view of Juno as it rotates with the planet. The emission at the frequency of 100.16 kHz shown in Figure 15, is from the same source as each emission is separated by ten hours. This emission lasts for four rotations (as there are four observed emissions separated by ten hours), however the fourth emission is not displayed in Figure 15 as it has relatively weak intensity in comparison to the others.

During the same burst, the 79.468 kHz frequency band was observed to have numerous emission events during the ten hour window. What this likely means is that there is more than one active source of emission at different longitudes. Hence, emission can be observed more than once during a rotation of Jupiter.

The second burst of this compression again exhibited the ten hour periodicity, thus it can be inferred that the source is longitudinally fixed. In this burst however, the frequency of the emission changes with each rotation. As can be seen in appendix F, in the first two rotations the emission is of lower frequencies (50.171kHz and 63.171 kHz), in the third and fourth however, the frequency shifts to 89.172 kHz and 100.16 kHz and becomes less intense. The decrease in intensity means that the mechanism that triggered the emission is not present anymore. The shift in frequency from lower to higher is due to the fact that nKom is thought to be emitted at the plasma frequency, as the plasma frequency depends on the plasma density, this shift in frequency likely means that the source of emission has moved to a location of higher plasma density in the Io torus. In the last burst during this compression (Figure 16), a similar case to the first burst is present. Four bands of frequency emitting at the same time with ten hour periodicity are observed meaning it can be inferred that one source, fixed in longitude is responsible for this emission. This burst appears to last for 10 rotations of Jupiter, with a gap of approximately 20 hours in between the fifth and sixth emission. As the intensity trend over all the frequency bands is decreasing before this gap, and increasing after it, it is possible that there is an emission present between the fifth and sixth emission but it is of very small relative intensity and thus was not detected. The decrease of intensity followed by an increase likely means that the emission mechanism was activated again after the initial activation.

In the third compression, three main bursts of emission are also observed. The first burst of this compression (appendix G), was unlike the previous bursts. Although it did exhibit a rough ten hour periodicity, the emission events were longer than that of the emissions previously observed. This burst also displayed a frequency shift as it rotated with Jupiter. The first two emissions were of primarily lower frequency bands and were twice as intense as the three that followed, which were composed of higher frequencies. Due to the period of the emissions, it can be concluded that all 5 emissions share the same source. The nature of the emission of this source leads to the conclusion that it began emitting at lower frequency and higher intensity and decreased in intensity and

increased in frequency with each rotation. Again this indicates that the source of the emission moved to a location with higher plasma density.

The second burst during this compression was the opposite of it's predecessor. From observing appendix I, the first five emissions seem to share the same source. In the time between the second and third emission, there are another two emissions that are likely from a different source to the others. The first three of the five emissions have higher frequencies then the following two and are also more intense (the second emission being the most intense). The pattern here appears to be that the frequency and intensity of the emission begin to decrease after the second rotation. As the frequency is decreasing with each emission the source is likely moving to an area of lower plasma density. Six hours after the final emission, a different source appears emitting high frequency and high intensity nKom (approximately $1.75 \times 10^{-13} W \cdot m^{-2} \cdot Hz^{-1}$). This source does not emit anything after this. This final emission suggests that the emission mechanism was activated and then rapidly deactivated, resulting in one relatively intense emission.

The third and final burst of this compression again seems to exhibit the behavior of a single fixed longitude source. The emission lasts for a total of eight rotations with its most intense emission occurring during its fourth and fifth rotations. The frequency is mostly of higher bands throughout, although the initial two emissions are composed of frequencies as low as 39.917 kHz and as high as 141.54 kHz. The following seven emissions are all between 100.16 kHz and 141.54 kHz. After the ninth and final emission there is a gap of approximately thirty hours before two more emissions are observed. As the gap between emission here corresponds to three rotations, it is likely that this is the same source.

The fourth and final compression consists of two bursts. The first burst appears to last for nine rotations following a general trend of decreasing intensity until the ninth emission which is composed of higher frequencies and more intense than the previous emissions. This suggests that the emission mechanism was reactivated and that the source moved to a location of higher plasma density inside the tours. The emissions after this no longer display ten hour periodicity, suggesting the activation of another source. The second burst in this compression occurs twenty hours after the first and displays the behaviour of a single emission source. The source emits for five rotations and the frequency of the

emission is relatively constant throughout. The intensity decreases after the first emission but increases in the fourth emission, again indicating the reactivation of the source.

In general, it is common to see the activation of nKom emission sources during a period of magnetospheric compression. The emissions tend to happen in bursts, with two or three bursts of emission during a compression. Typically, a burst of emission will last for a number of rotations, generally decreasing in intensity unless the source is reactivated. It is common for the frequency of the emission to change over the course of a number of rotations. In this study, there have been instances observed when the frequency increases with time and instances when it decreases. As mentioned, this is as a result of the emission source changing location in the torus. The second and third compression identified in this study were stronger than the fourth, (the dynamic pressure of the second and third was 0.270 nPa and 0.267 nPa respectively, whereas the fourth was 0.215 nPa). This was evident in the emission as the emission during the second and third compressions reached intensities of $1.75 \times 10^{-13} W \cdot m^{-2} \cdot Hz^{-1}$, whereas during the fourth compression the intensity reached a maximum of $1 \times 10^{-13} W \cdot m^{-2} \cdot Hz^{-1}$.

5 Conclusions

Using the findings from Hospodarsky et al. (2017), and the Joy et al. model, four periods of magnetospheric compression have been identified during Juno's approach and first three orbits of Jupiter. The Jovian nKom emission has been analysed during each of these periods of compression and it has been determined that compression of Jupiter's magnetosphere by the solar wind results in the activation of nKom sources. During periods of compression, nKom emissions typically display ten hour periodicity as a result of the source being longitudinally fixed, and rotating with Jupiter. The frequency of emission is found to be subject to change, as the source moves into locations of higher and lower plasma density in the torus, the frequency of the emission changes accordingly.

Further work in this area may include the study of further Juno orbits past the initial three in order to identify more periods of magnetospheric compression, as well as examining the periodicity of the nKom emission more closely. Moreover, the findings presented in this study imply that future studies could use nKom emission as a proxy for the solar wind conditions at Jupiter.

6 References

- ALFVÉN, H., 1942. Existence of Electromagnetic-Hydrodynamic Waves. *Nature*, 150(3805), pp.405-406.
- Bagena, F. and Bartlett, S., n.d. [image] Available at: [\[https://lasp.colorado.edu/home/mop/files/2012/04/JupMag-8W1.jpg\]](https://lasp.colorado.edu/home/mop/files/2012/04/JupMag-8W1.jpg); [Accessed 19 January 2022].
- Bridgman, T., 2017. SVS: Alfvén Waves - Basic. [online] Svs.gsfc.nasa.gov. Available at: [\[https://svs.gsfc.nasa.gov/4560\]](https://svs.gsfc.nasa.gov/4560); [Accessed 7 January 2022].
- Faden, J., Weigel, R., Merka, J. and Friedel, R., 2010. Autoplot: a browser for scientific data on the web. *Earth Science Informatics*, 3(1-2), pp.41-49.
- Hess, S., Echer, E., Zarka, P., Lamy, L. and Delamere, P., 2014. Multi-instrument study of the Jovian radio emissions triggered by solar wind shocks and inferred magnetospheric subcorotation rates. *Planetary and Space Science*, 99, pp.136-148.
- Hess, S., Echer, E. and Zarka, P., 2012. Solar wind pressure effects on Jupiter decametric radio emissions independent of Io. *Planetary and Space Science*, 70(1), pp.114-125.
- Hospodarsky, G., Kurth, W., Bolton, S., Allegrini, F., Clark, G., Connerney, J., Ebert, R., Haggerty, D., Levin, S., McComas, D., Paranicas, C., Rymer, A. and Valek, P., 2017. Jovian bow shock and magnetopause encounters by the Juno spacecraft. *Geophysical Research Letters*, 44(10), pp.4506-4512.
- Jackman, C., Thomsen, M. and Dougherty, M., 2019. Survey of Saturn's Magnetopause and Bow Shock Positions Over the Entire Cassini Mission: Boundary Statistical Properties and Exploration of Associated Upstream Conditions. *Journal of Geophysical Research: Space Physics*, 124(11), pp.8865-8883.
- Jones, C., 2018. Jupiter's magnetic field revealed by the Juno spacecraft. *Nature*, 561(7721), pp.36-37.

Joy, S., Kivelson, M., Walker, R., Khurana, K., Russell, C. and Ogino, T., 2002. Probabilistic models of the Jovian magnetopause and bow shock locations. *Journal of Geophysical Research*, 107(A10).

Louarn, P., Roux, A., Perraut, S., Kurth, W. and Gurnett, D., 1998. A study of the large-scale dynamics of the Jovian magnetosphere using the Galileo Plasma Wave Experiment. *Geophysical Research Letters*, 25(15), pp.2905-2908.

Louis, C., 2021. STELLAR SWW: Magnetospheric Radio Emission. [video] Available at: https://www.youtube.com/watch?v=YR00L2ov_iI [Accessed 25 November 2021].

C. K. Louis, P. Zarka and B. Cecconi (2021a). Juno/Waves estimated flux density Collection (Version 1.0) [Data set]. PADC. <https://doi.org/10.25935/6jg4-mk86>

C. K. Louis, P. Zarka and B. Cecconi (2021b). Catalogue of Jupiter radio emissions identified in the Juno/Waves observations (Version 1.0) [Data set],PADC, <https://doi.org/10.25935/nhb2-wy29>

Ogino, T., Walker, R. and Kivelson, M., 1998. A global magnetohydrodynamic simulation of the Jovian magnetosphere. *Journal of Geophysical Research: Space Physics*, 103(A1), pp.225-235.

Peale, S., Cassen, P. and Reynolds, R., 1979. Melting of Io by Tidal Dissipation. *Science*, 203(4383), pp.892-894.

Ryden, B., 2009. [online] Astronomy.ohio-state.edu. Available at: <https://www.astronomy.ohio-state.edu/ryden.1/ast825/ch11.pdf> [Accessed 8 January 2022].

Scied.ucar.edu. 2012. The Sun's Corona (Upper Atmosphere) — Center for Science Education. [online] Available at: <https://scied.ucar.edu/learning-zone/sun-space-weather/solar-corona> [Accessed 4 January 2022].

Swpc.noaa.gov. 2017. Coronal Mass Ejections — NOAA / NWS Space Weather Prediction Center. [online] Available at: <https://www.swpc.noaa.gov/phenomena/coronal-mass-ejections> [Accessed 6 January 2022].

Young, D., 2011. A brief introduction to fluid mechanics. Hoboken, NJ: Wiley.

7 Appendices

7.1 A - Boundary Crossing Determination

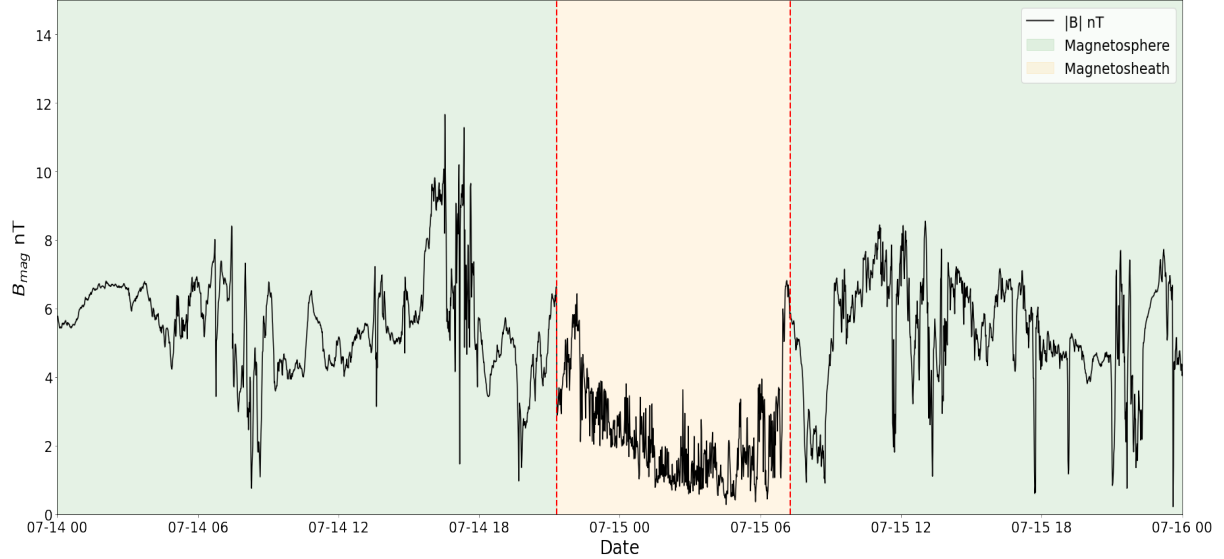


Figure 18: The magnitude of the Jovian magnetic field from 14/07 (DOY 196) until the end of 16/07 (DOY 197). Here the magnetic field magnitude has been used to determine the region at which the spacecraft crosses a boundary

7.2 B - Initial Juno Orbital Path XZ Plane

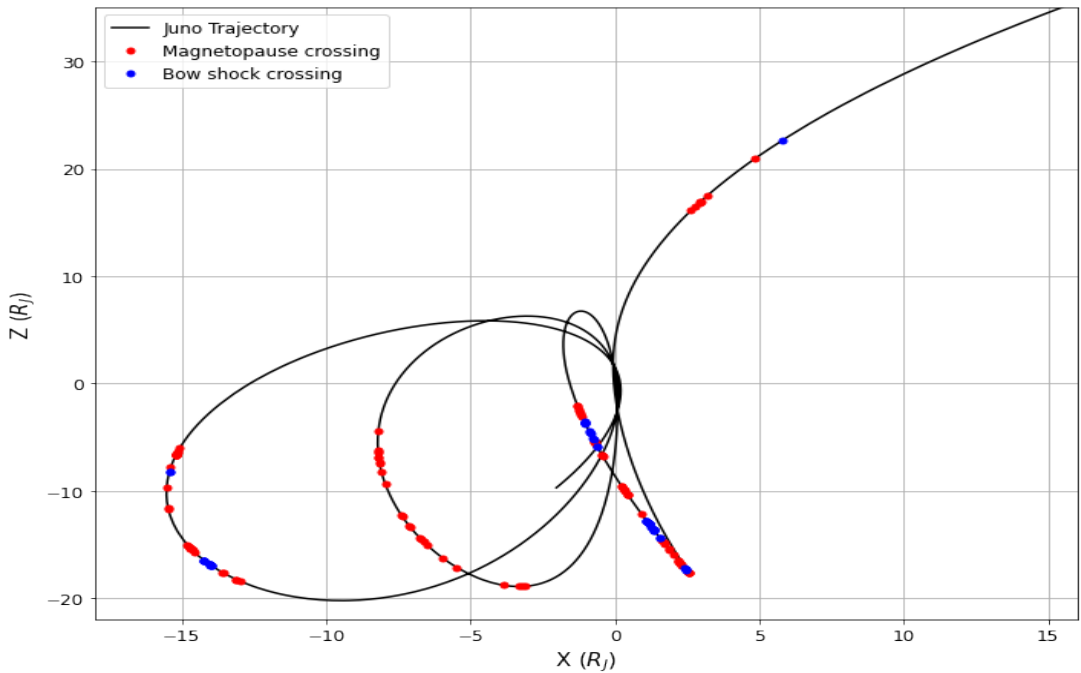


Figure 19: The orbital path of the Juno spacecraft for its approach to Jupiter and its first three orbits in the XZ plane (black line). Plotted onto this is the position the spacecraft crossed the magnetopause (red dots) and the bow shock (blue dots) boundaries.

7.3 C - An Example of the Joy et al. Model Creating Surfaces

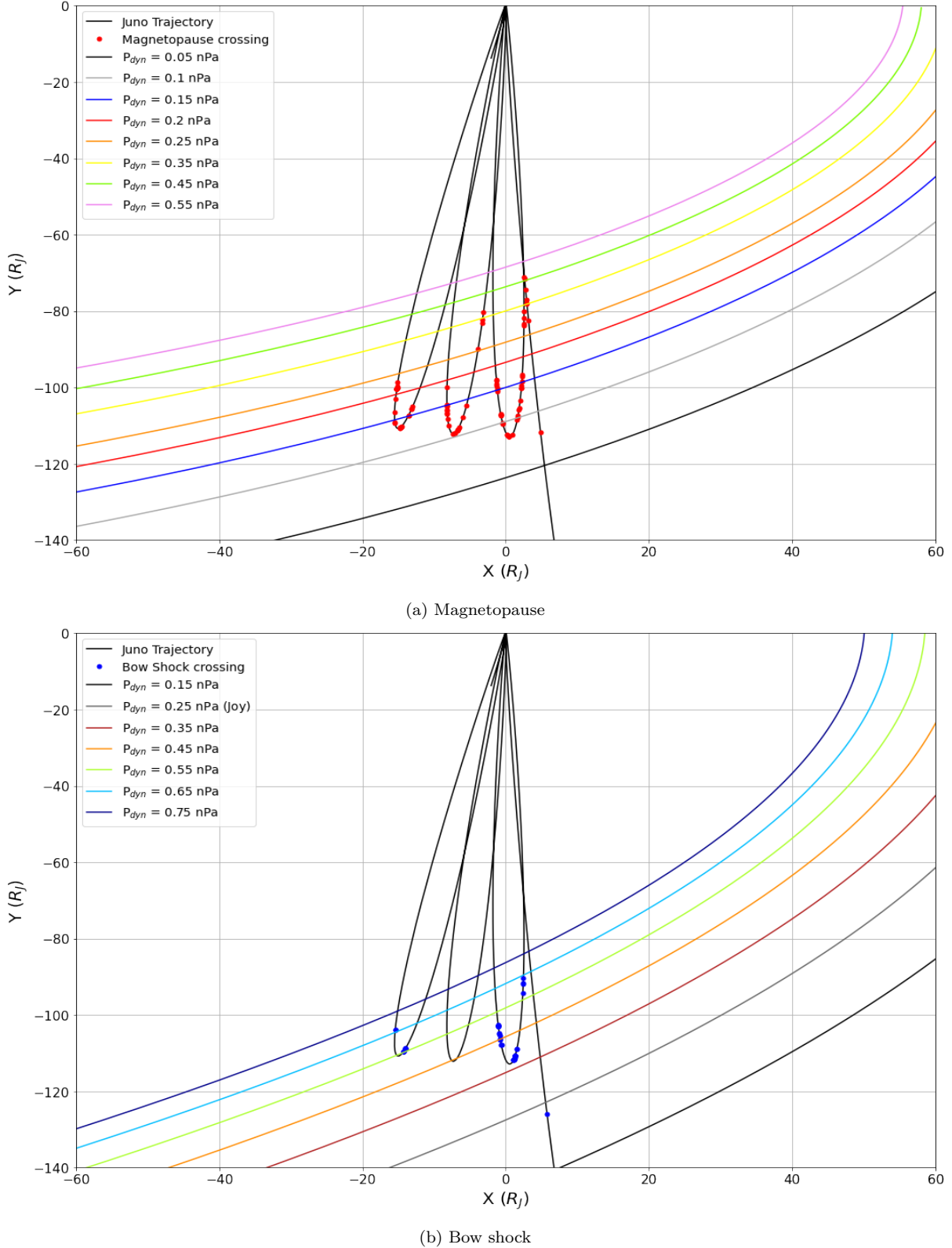


Figure 20: Two figures of the Juno orbital path including the magnetopause (top) and bow shock crossing locations (bottom). On plot (a) is a number of magnetopause surfaces representing the according values of dynamic pressure. Plot (b) contains bow shock surfaces corresponding to a value of dynamic pressure. These surfaces have been obtained using the Joy et al. model.

7.4 D - Initial Juno Orbital Path in Three Dimensions

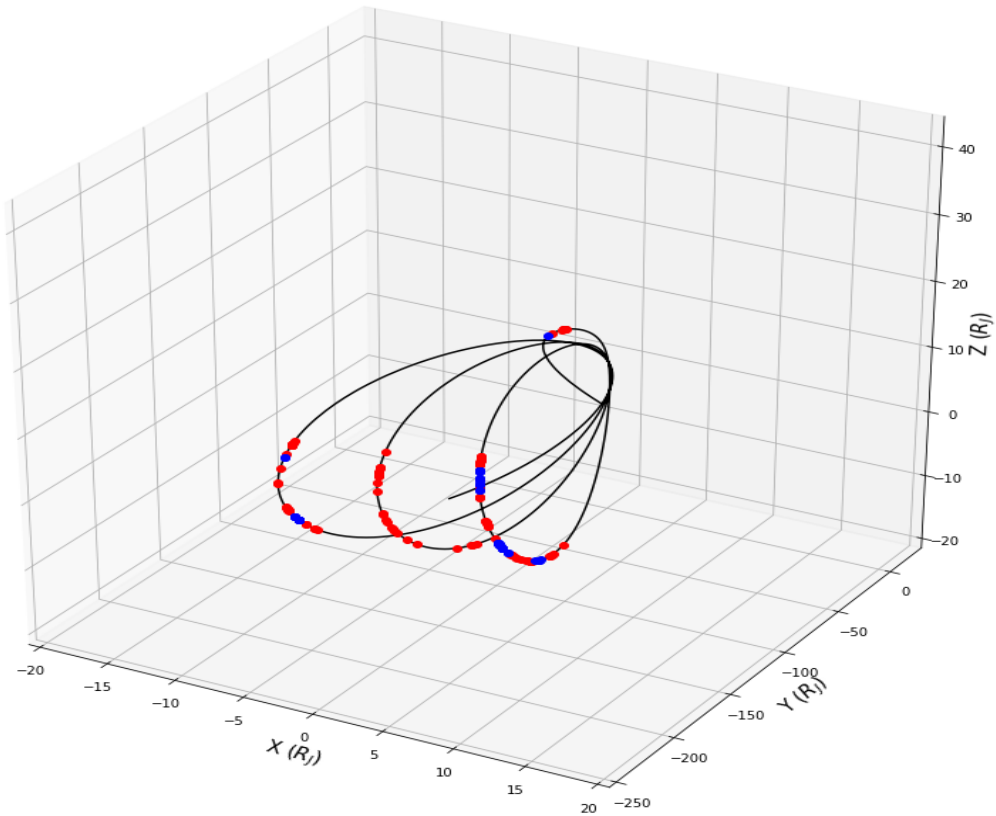


Figure 21: A 3D plot of the Juno orbital path (black line) along with the position the spacecraft crossed the magnetopause (red dots) and the bow shock (blue dots) boundaries.

7.5 E - nKom Emission for 1st Compression Period DOY 180 - 182

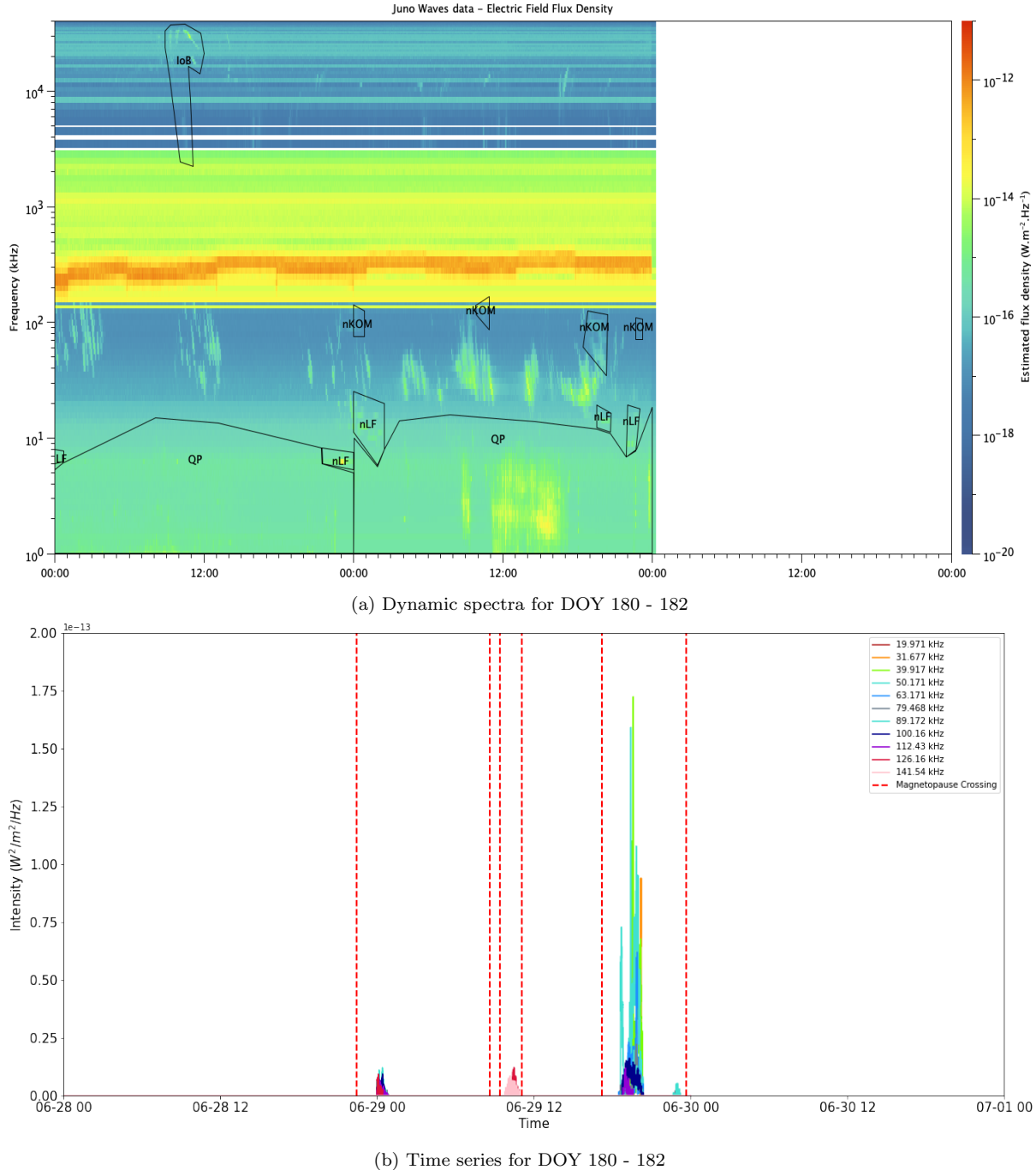


Figure 22: (a) The dynamic spectra and time series for the first identified compression period (DOY 180 - 182). The Juno-Waves was turned off on DOY 182 during orbit insertion, hence there is data recorded after the end of DOY 181.

7.6 F - Second Burst of Emission During the Second Identified Compression

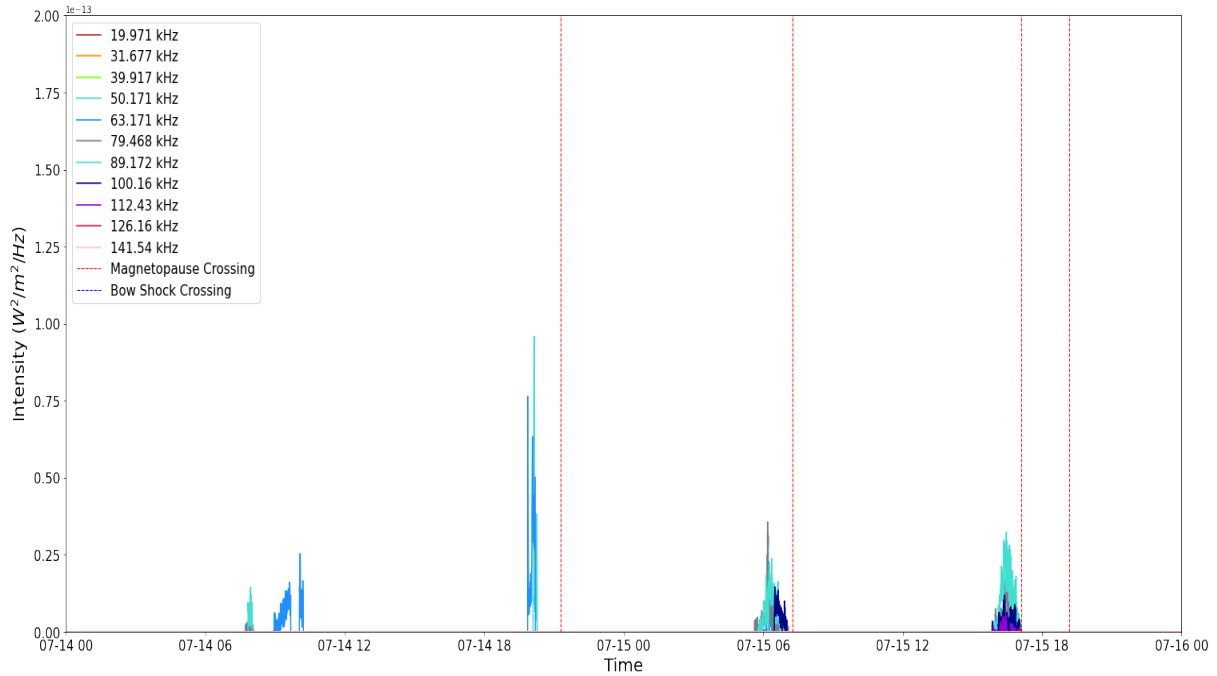


Figure 23: Time series for second emission burst during second identified compression from DOY 194 to DOY 195.

7.7 G - First Burst of Emission During the Third Identified Compression

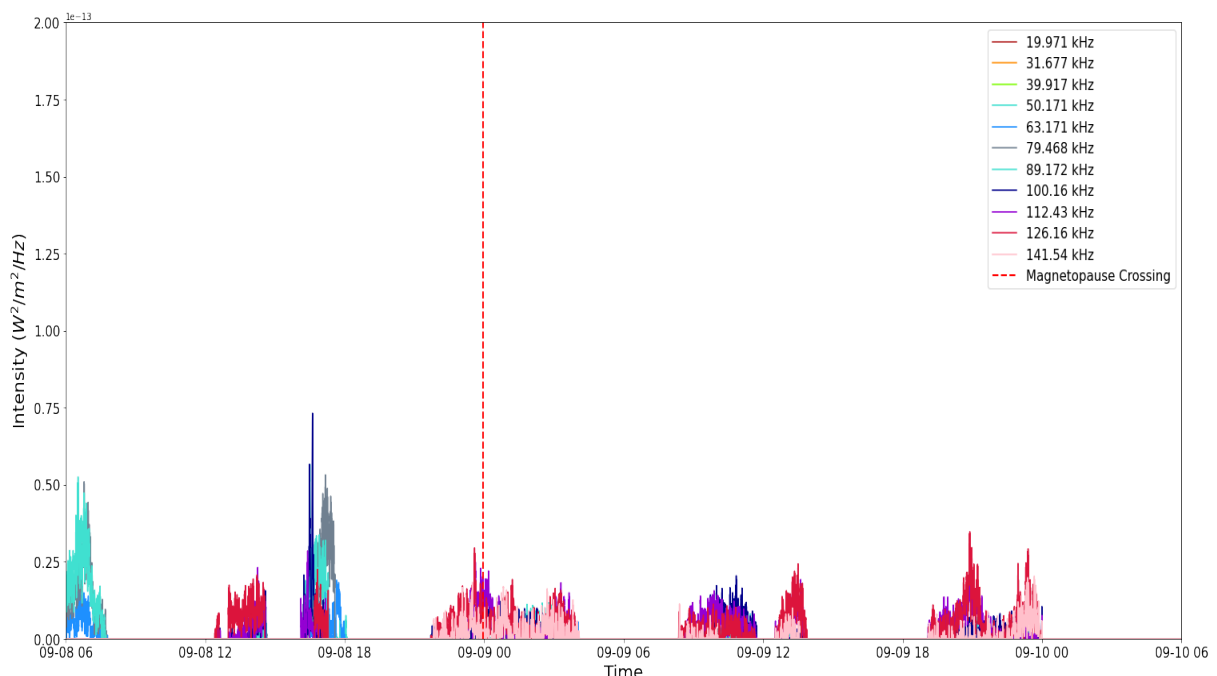


Figure 24: Time series for first emission burst during third identified compression from DOY 252 to DOY 253.

7.8 H - Third Burst of Emission During the Third Identified Compression

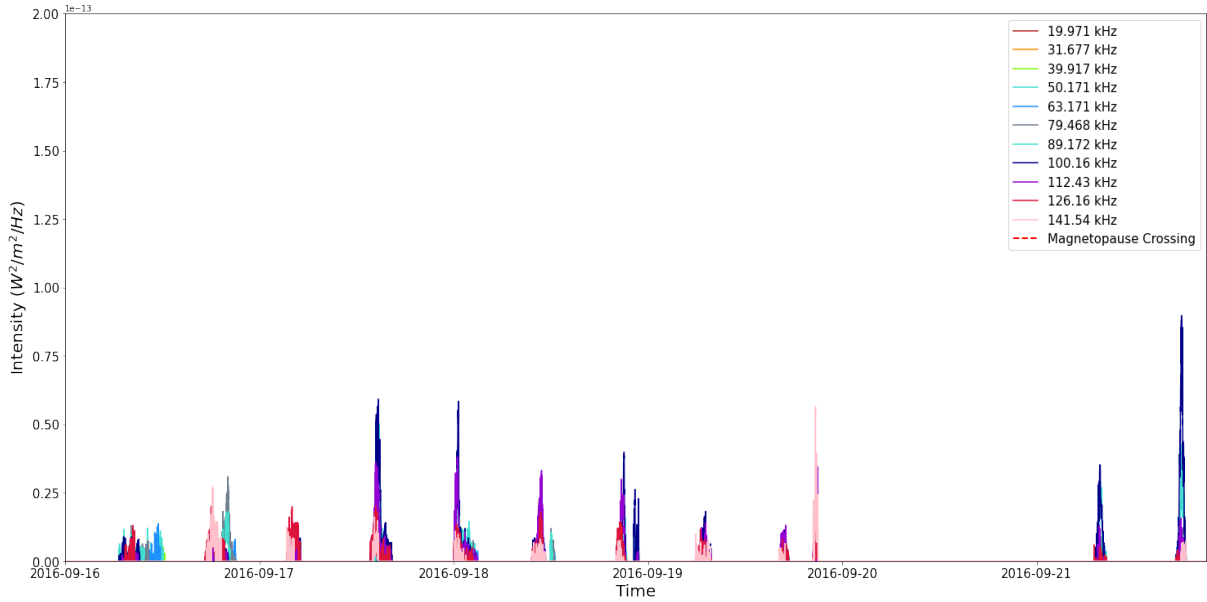


Figure 25: Time series for third emission burst during third identified compression from DOY 260 to DOY 265.

7.9 I - Time Series for Second Emission During Third Compression From DOY 256 to DOY 258

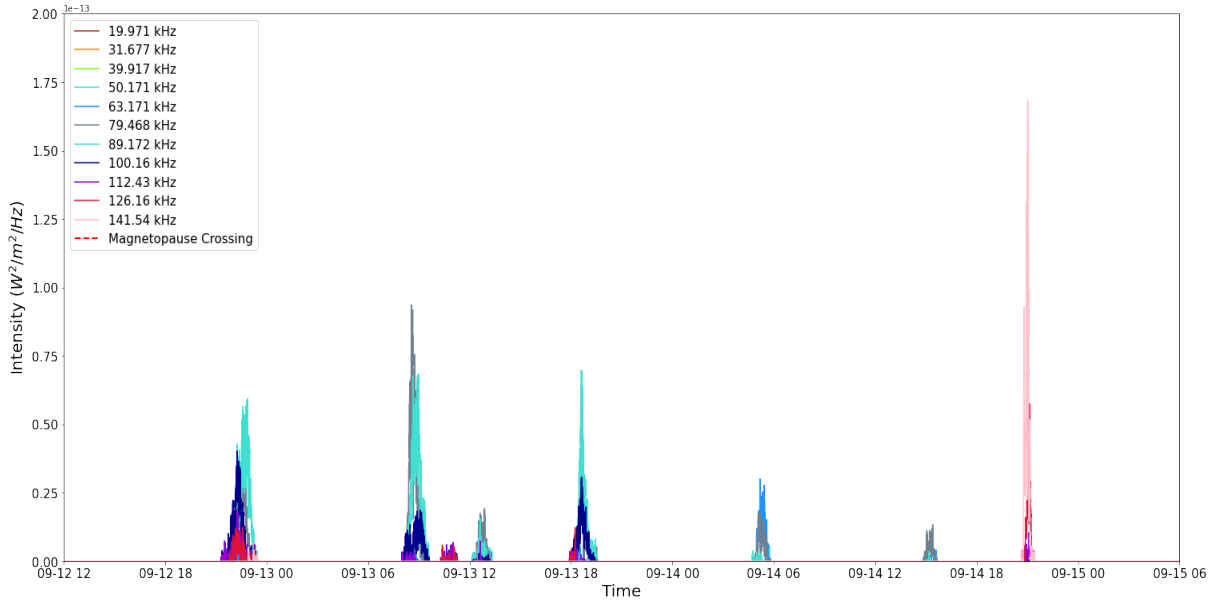


Figure 26: Time series for second emission burst during third identified compression from DOY 256 to DOY 258.

7.10 J - nKom Emission During Fourth Compression DOY 276

- 297

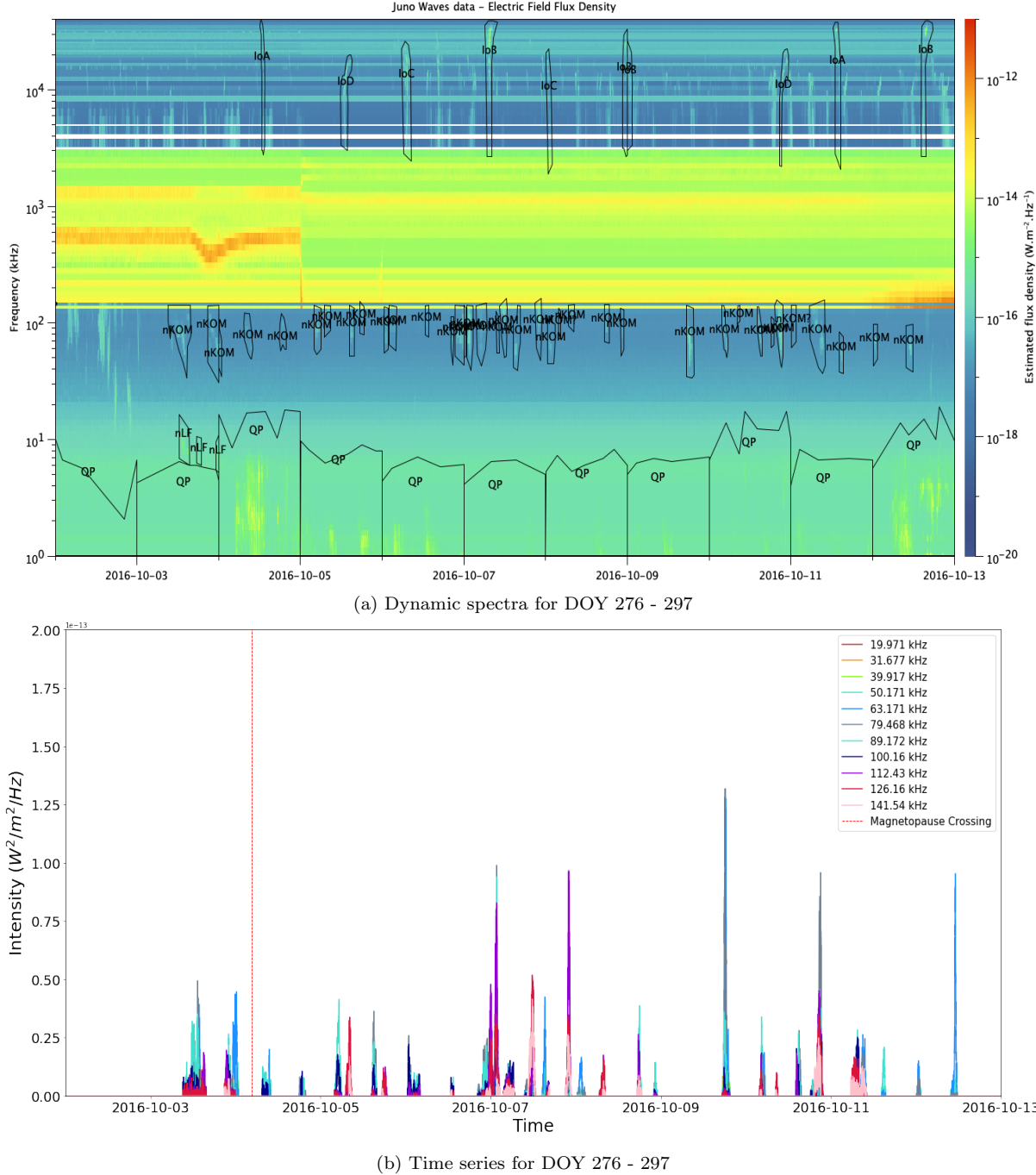


Figure 27: The dynamic spectra and time series for the fourth identified compression period (DOY 180 - 182).